The endoplasmic reticulum and casein-containing vesicles contribute to milk fat globule membrane

Edith Honvo-Houéto[a,†], Céline Henry[b], Sophie Chat[a,‡], Sarah Layani[a,§], and Sandrine Truchet[a,†,*]
[a]INRA, UR1196 Génomique et Physiologie de la Lactation, F-78352 Jouy-en-Josas Cedex, France; [b]INRA, UMR1319, MICALIS, PAPPSO, F-78352 Jouy-en-Josas Cedex, France

ABSTRACT **During lactation, mammary epithelial cells secrete huge amounts of milk from their apical side. The current view is that caseins are secreted by exocytosis, whereas milk fat globules are released by budding, enwrapped by the plasma membrane. Owing to the number and large size of milk fat globules, the membrane surface needed for their release might exceed that of the apical plasma membrane. A large-scale proteomics analysis of both cytoplasmic lipid droplets and secreted milk fat globule membranes was used to decipher the cellular origins of the milk fat globule membrane. Surprisingly, differential analysis of protein profiles of these two organelles strongly suggest that, in addition to the plasma membrane, the endoplasmic reticulum and the secretory vesicles contribute to the milk fat globule membrane. Analysis of membrane-associated and raft microdomain proteins reinforces this possibility and also points to a role for lipid rafts in milk product secretion. Our results provide evidence for a significant contribution of the endoplasmic reticulum to the milk fat globule membrane and a role for SNAREs in membrane dynamics during milk secretion. These novel aspects point to a more complex model for milk secretion than currently envisioned.**

Monitoring Editor
Patrick J. Brennwald
University of North Carolina

Received: Jun 6, 2016
Revised: Aug 3, 2016
Accepted: Aug 3, 2016

INTRODUCTION

The mammary gland is dedicated to the feeding of the mammalian newborn. Therefore this organ undergoes repeated cycles of growth, differentiation, and regression concomitantly with variations in the reproductive status. During lactation, highly differentiated mammary epithelial secretory cells (MESCs) are organized into alveolar structures that are surrounded by contractile myoepithelial cells and embedded in a stroma (connective and adipose tissues, blood vessels, and nerve terminals). MESCs produce and secrete large amounts of milk, which is an aqueous fluid containing proteins (mainly caseins, assembled in micellar structures), milk fat globules (MFGs), and soluble components, such as lactose and minerals. Caseins are synthesized and transported along the secretory pathway and released by exocytosis. Although casein secretion appears to be mostly continuous, MESCs possess both a constitutive and a regulated secretory pathway (Turner *et al.*, 1992). Whatever their secretory mode, trafficking steps within the secretory pathway and exocytosis, that is, the fusion of casein-containing vesicles with the apical plasma membrane (APM), involve soluble *N*-ethylmaleimide–sensitive fusion (NSF) attachment protein receptor (SNARE) proteins (Chat *et al.*, 2011), as described in other cell types (Sollner *et al.*, 1993b; Jahn and Scheller, 2006). The various SNAREs predominantly reside in distinct cellular compartments and are involved in specific trafficking pathways, with SNARE pairing potentially contributing to the specificity of the membrane fusion events (McNew, 2008). By zipping through their coil-coiled domains, R-SNAREs (formerly termed v-SNAREs), present in the vesicle membrane, associate with Q-SNAREs (formerly termed t-SNAREs), localized on

This article was published online ahead of print in MBoC in Press (http://www.molbiolcell.org/cgi/doi/10.1091/mbc.E16-06-0364) on August 17, 2016.

The authors declare that they have no conflicts of interest.

S.T. conceived and designed the project. C.H. performed LC-MS/MS experiments and helped to interpret the results. S.C. performed electron microscopy and helped to interpret the results. E.H.H., S.L., and S.T. performed all other experiments and analyzed data. S.T. wrote the manuscript.

Present addresses: †INRA, UMR 1313 GABI, Génomique Fonctionnelle et Physiologie de la Glande Mammaire, F-78352 Jouy-en-Josas, France; ‡CNRS UMR 6290 IGDR, Translation and Folding Team, Université de Rennes 1, 35042 Rennes Cedex, France; §UPMC Université Paris 06, ERL INSERM U1057/UMR7203, Faculty of Medicine Pierre et Marie Curie, CHU Saint-Antoine, F-75012 Paris, France.

*Address correspondence to: Sandrine Truchet (sandrine.truchet@jouy.inra.fr).

Abbreviations used: APM, apical plasma membrane; BTN1, butyrophilin; CH, cholesterol; CLD, cytoplasmic lipid droplet; ER, endoplasmic reticulum; IIF, indirect immunofluorescence; MESC, mammary epithelial secretory cell; MFGM, milk fat globule membrane; PLIN2, perilipin2; PM, plasma membrane; SNAP, synaptosomal-associated protein; SNARE, soluble *N*-ethylmaleimide–sensitive factor attachment protein receptor; SV, secretory vesicle; VAMP, vesicle-associated membrane protein.

the target membranes, to form a highly stable four-helix bundle complex termed the SNARE complex. This complex then gradually brings the two opposing lipid bilayers into close proximity and promotes their fusion (Sollner *et al.*, 1993b; Weber *et al.*, 1998). Afterward, SNARE complexes are dissociated by the NSF adenosine triphosphatase and its adaptor protein synaptosomal-associated protein (SNAP; Sollner *et al.*, 1993a). Previous work suggests that at the least SNAP23, vesicle-associated membrane protein 8 (VAMP8), and syntaxins (Stx) 7 and 12 play a role in casein exocytosis (Wang *et al.*, 2007; Chat *et al.*, 2011). Some SNARE proteins have also been localized to membrane microdomains called lipid rafts, which are small, heterogeneous, highly dynamic, and sterol and sphingolipid enriched. Owing to their composition, lipid rafts are believed to display a liquid-ordered phase with a reduced molecular diffusion, thus specifically segregating some membrane proteins. By locally clustering and stabilizing protein–lipid and protein–protein interactions, lipid rafts both compartmentalize and optimize signaling efficiency and also favor membrane curvature. Lipid rafts are present along the secretory pathway and at the plasma membrane (PM) and have been implicated in a wide range of cellular processes, including T- and B-cell activation, hormone signaling, focal adhesions and cell migration, membrane trafficking in polarized epithelial cells and exocytosis (for reviews, see Lang, 2007; Lingwood and Simons, 2010; Simons and Sampaio, 2011).

Although different mechanisms have been proposed, the prevailing model is that cytoplasmic lipid droplets (CLDs) are formed by accumulation of neutral lipids (mainly triacylglycerols and sterol esters) and cholesterol (CH) between the two leaflets of the endoplasmic reticulum (ER) membrane (Wilfling *et al.*, 2014). Therefore CLDs are surrounded by a CH-containing phospholipid monolayer that is compositionally distinct from ER membranes or sphingolipid/CH-rich microdomains (Tauchi-Sato *et al.*, 2002; Bartz *et al.*, 2007). Numerous mass spectrometry (MS) studies have established a panel of specific CLD-associated proteins, including enzymes involved in lipid metabolism, perilipins (PLIN1, PLIN2/adipophilin/adipocyte differentiation–related protein, PLIN3/tail-interacting protein of 47 kDa [TIP47]), members of the cell death–inducing DNA fragmentation factor 45–like effector (CIDE) protein family (CIDE-A–C), and Rab18 GTPase. In addition, ER-resident proteins, some of which are required for CLD formation and/or expansion, have also been repeatedly identified in CLD preparations. Moreover, proteins usually associated with other cellular compartments, such as the Golgi apparatus, endosomes, peroxisomes, mitochondria, and the PM, are also found in CLDs, reflecting their highly dynamic interactions with these organelles (for recent reviews, see Barbosa *et al.*, 2015; Gao and Goodman, 2015). Furthermore, these interactions are regulated by some Rab GTPases found in CLDs and promote both protein and lipid transfer and/or metabolism between cellular compartments (Kiss and Nilsson, 2014). In some cell types, such as MESCs, large CLDs are formed, at least in part, by fusion of smaller CLDs. Although the mechanism of CLD fusion is still a matter of debate, some SNARE proteins were found in purified CLDs, and SNAP23 was shown to be involved in their growth by fusion (Bostrom *et al.*, 2007). CLDs are believed to bud from the ER but may stay connected to the ER as a specialized ER subdomain. Whatever the case, CLDs appear to remain intimately associated with the ER and contact points between CLDs, and ER cisternae appear to be ribosome rich (Wan *et al.*, 2007). In lactating MESCs, CLDs are vectorially transported to the apical side, where they are secreted as large MFGs (Mather and Keenan, 1998; Heid and Keenan, 2005; McManaman, 2012). MFGs represent a unique feature of lipid secretion because they are released surrounded by a phospholipid monolayer arising from the ER and enwrapped by another phospholipid bilayer coming from the APM. Although several models have been proposed for MFG secretion, the molecular mechanisms and the kinetics of this event are still controversial (Jeong *et al.*, 2013). Numerous MS analyses of the MFG membrane (MFGM) have led to the identification of several major proteins, such as butyrophilin (BTN1; Ogg *et al.*, 2004), xanthine oxidoreductase (XOR; Vorbach *et al.*, 2002), CIDE-A (Wang *et al.*, 2012), and PLIN2 (Chong *et al.*, 2011), the role of which has been functionally demonstrated in MFG secretion. Two central questions remain: the origin of the membrane needed for MFG release, and the molecular mechanisms underlying this process. Because the diameter of MFGs is ~0.5–10 µm, depending on the species, and due to the high number of MFGs secreted during lactation, the membrane surface needed could exceed that of the APM of MESCs.

In the present study, we asked whether the MFGM arises only from the APM or whether other intracellular compartments contribute to its formation and, if so, to what extent. We assumed that the differential analysis of protein profiles from CLDs and MFGs obtained by large-scale proteomics would lead to "protein signatures" of intracellular compartments that contribute to the MFGM formation. Indeed, our results show that membranous compartments such as the ER, secretory vesicles (SVs), and mitochondria provide membranes during MFG budding. This possibility is also supported by the specific analysis of the transmembrane proteins and the patterns of SNARE proteins associated with each of these cellular compartments. Of interest, free CH and GM1 ganglioside, two known components of lipid rafts, appear closely associated with CLDs and MFGs. In agreement with this, the analysis of raft-associated proteins clearly showed that they represent up to 50% of the proteins identified in CLDs, whereas this proportion appeared slightly reduced in MFGMs, suggesting that lipid rafts associate early with the fat fraction of milk. Thus the present work points to the existence of a specialized mechanism for connecting intracellular membranes during milk product secretion.

RESULTS

The differential analysis of CLD and MFGM proteins identifies major functions and intracellular compartments involved in their biogenesis and secretion

To identify the proteins differentially associated with CLDs and secreted MFGs, we performed a large-scale proteomics analysis of these two supramolecular structures by liquid chromatography–tandem mass spectrometry (LC-MS/MS). The experimental strategy is shown in Figure 1. CLDs were prepared from mammary acini purified from mouse mammary glands at day 10 of lactation (L10), and MFGMs were isolated from mouse milk collected at the same lactation stage. We first checked the purity of the isolated fractions. The preparation of CLDs (Figure 2A) was first analyzed by light and fluorescence microscopy (Figure 2B). Purified CLDs appeared as small, spherical structures of heterogeneous but limited diameters (Figure 2B, nt), similar to CLDs isolated from other cell types (Liu *et al.*, 2004; Bartz *et al.*, 2007). Of importance, CLDs counterstaining for glycoconjugates (Figure 2B, GC) or F-actin (Figure 2B, actin) clearly showed that membrane debris, other cellular organelles, or actin were barely detected in our preparation. Conversely, CLDs counterstaining for GM1 ganglioside (Figure 2B, GM1) revealed that membrane rafts were closely linked to CLDs, as also suggested by our other results (see later description). We further verified the purity of our CLD preparation by Western blot. Equal amounts (50 µg) of P1, S1, total membrane (P2), cytosol (S2), and CLDs fractions were separated by SDS–PAGE and analyzed using the indicated antibodies.

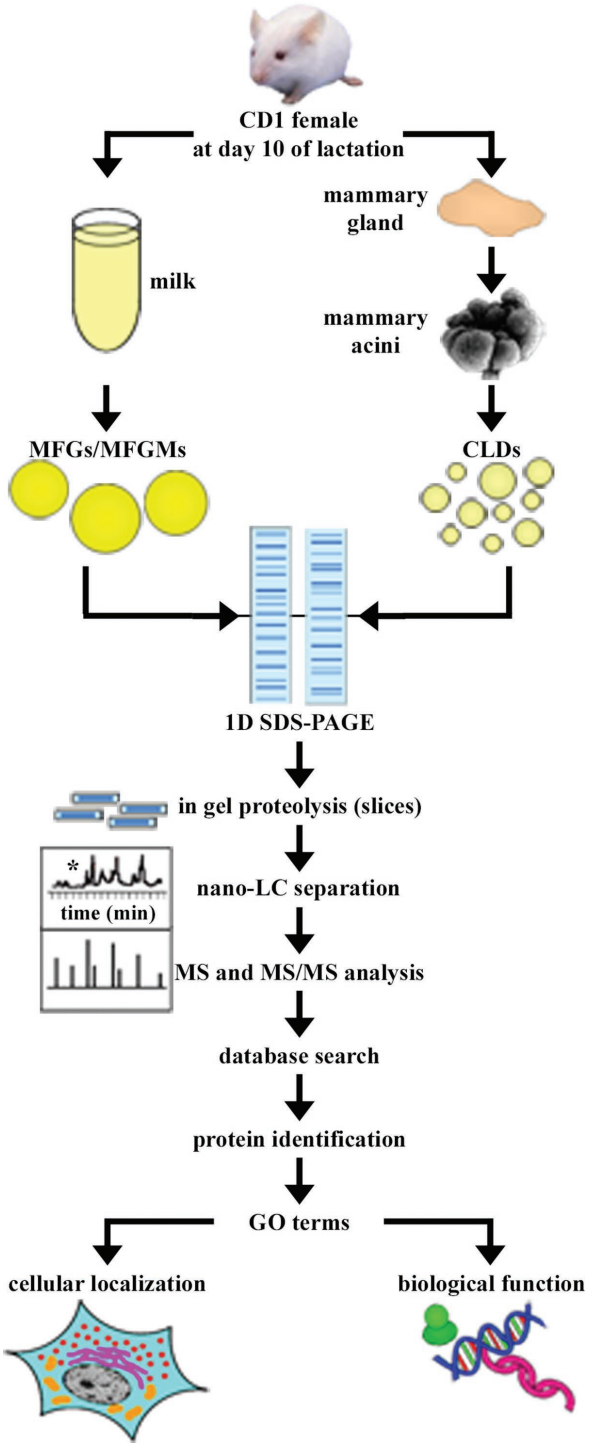

FIGURE 1: Experimental flowchart for the identification of the proteins associated with murine MESC CLDs and with MFGMs. MFGs were isolated from mouse milk (L10), and MFGM proteins were extracted. MESCs (acini) were purified from mouse mammary glands collected at L10 and homogenized, and CLDs were purified by flotation on a sucrose gradient. Proteins from both CLDs and MFGMs were separated by 1D SDS–PAGE. The gel lanes were sliced into 26 pieces, the proteins were subjected to in-gel trypsin digestion, and the hydrolysates were analyzed by LC-MS/MS. The proteins identified by at least two peptides were classified for both function and cellular localization based on their GO terms (Uniprot KB database).

Figure 2C clearly shows that 1) the protein pattern of purified CLDs was significantly different from that of the other cellular fractions (Figure 2C, CLDs), 2) the isolated CLDs had little to no contamination with plasma membrane (E-cadherin), ER lumen (PdiA3, GRP78), ER membrane (calnexin, Stx18), Golgi (GM130), or cytosol (β-actin), and 3) the CLD fraction was significantly enriched for PLIN2, a specific marker of CLDs (Figure 2D, CLDs). In addition, the protein profiles of various CLD preparations were almost identical, indicating the reproducibility and quality of the purification method (unpublished results).

To ensure the quality of the MFGM samples, we first analyzed proteins from the whole–mouse milk and milk subfractions, namely caseins, lactoserum, and MFGMs, by SDS–PAGE. The protein profile obtained for MFGMs appeared to contain only low levels of caseins and to be specifically enriched in some proteins (Figure 3, arrowheads) compared with whole milk, casein pellet, and lactoserum. MFGs and MFGMs were also observed by transmission electron microscopy after negative coloration. As shown in Figure 3B, MFGs appeared as large, round lipid droplets, whereas isolated MFGMs were less structured and clearly devoid of neutral lipid core, membrane debris, or cellular organelles, confirming the purity of the prepared MFGMs. MFGs have been reported to occasionally contain cytoplasmic crescents, the incidence of which varies by species, milking interval, and time of day (Patton and Huston, 1988; Huston and Patton, 1990). To estimate the incidence of these structures, we labeled MFGs isolated from freshly collected mouse milk at day 10 of lactation with acridine orange (AO), FM4-64, Alexa 594–conjugated wheat germ agglutinin (WGA), or rhodamine-conjugated phalloidin (Supplemental Figure S1). The incidence of cytoplasmic crescents was estimated to be 2.95, 2,91, 3,15, and 2.63% (average 2.91%) of the mouse MFGs labeled with AO (n = 5496), FM4-64 (n = 6662), WGA (n = 5528), or phalloidin (n = 5474), respectively. Thus the low incidence of cytoplasmic crescents in mouse MFGs would likely not affect the subsequent mass spectrometry analysis.

The one-dimensional (1D) protein profiles of both CLD and MFGM fractions that were subjected to proteomic analysis by LC-MS/MS were similar to published results and clearly show that major proteins, namely PLIN2 in CLDs and BTN1 and MFG-EGF factor 8/lactadherin (MFG-E8) in MFGMs, are specifically enriched in our preparations (Figure 4, arrowheads). Moreover, our LC-MS/MS results (see Supplemental Table S1 for protein and peptide identification) confirmed the purity of the analyzed fractions, as the major proteins detected were known protein markers of CLDs and MFGMs, respectively. The LC-MS/MS analysis of CLDs (Supplemental Table S1, CLD) led to the unambiguous identification of 260 proteins (peptide false discovery rate [FDR] = 0.09%) with an average recovery of ~40% with previously published studies (Wu *et al.*, 2000; Brasaemle *et al.*, 2004; Fujimoto *et al.*, 2004; Liu *et al.*, 2004; Turro *et al.*, 2006; Bartz *et al.*, 2007; Wan *et al.*, 2007; Hodges and Wu, 2010; Bouchoux *et al.*, 2011). Proteins commonly found in CLD preparations, such as PLIN2, Rab18, and enzymes involved in lipid metabolism (SDR1, ABHD5, NADH Cytb5 reductase), were identified, validating the procedure (see also Western blot results). Proteins were classified according to their function (Supplemental Table S1, CLD function) or cellular localization (Supplemental Table S1, CLD, localization) on the basis of a single relevant gene ontology (GO) term. Only two ribosomal proteins (0.77%; see later description) were identified in CLDs. Owing to the lack of relevance of this functional category and because it contain numerous hits, we systematically excluded ribosomal proteins from further statistical analyses so as not to introduce a bias in favor of the function and cellular

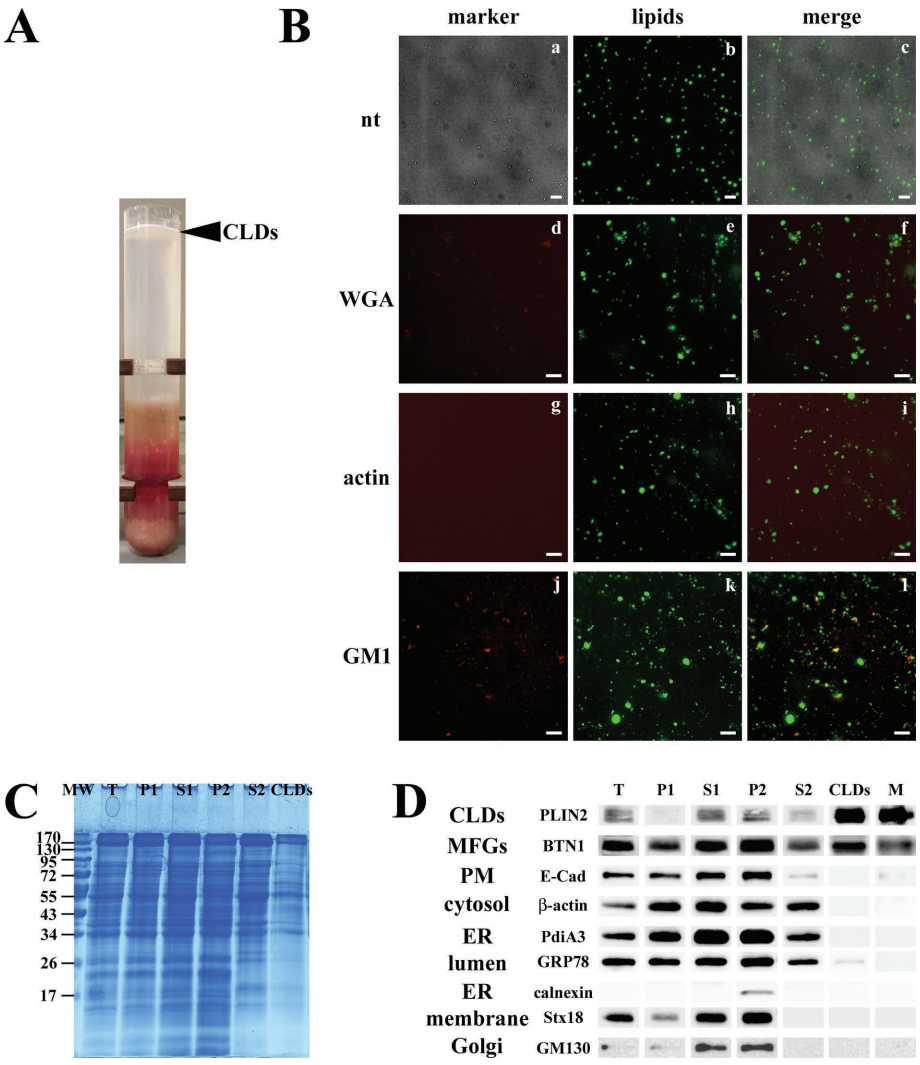

FIGURE 2: Isolation and quality of the purified CLDs from mouse lactating mammary gland. (A) Mammary acini purified from mouse mammary gland at day 10 of lactation were washed and homogenized. Total lysate (T) was centrifuged at 800 × *g* for 10 min at 4°C. The postnuclear supernatant (S1) was subsequently centrifuged at 110,000 × *g* for 1 h at 4°C to isolate cellular membrane (P2) and soluble material (S2). After centrifugation of the total lysate at 274,000 × *g* for 1 h at 4°C, the top white layer was the CLD fraction. (B) Isolated CLDs were analyzed by differential interference contrast microscopy (a; nt, not treated) and fluorescence microscopy after BODIPY 493/503 staining (lipids; b, e, h, k). CLDs were counterstained with Alexa Fluor 594–conjugated WGA (d), rhodamine-conjugated phalloidin (actin; g), or Alexa 594–conjugated CTxB (GM1; j) and merged (c, f, i, l) in order to visualize potential contaminations. Scale bar, 10 μm. (C) Proteins extracted from the different fractions were separated by SDS–PAGE and stained with Coomassie blue. Note the distinct banding pattern of CLDs. (D) The same protein samples were also subjected to Western blotting to test for contamination from other cellular fractions. Specific antibodies were used to probe for marker proteins of different cellular organelles/fractions: PLIN2 (CLD protein), BTN1 (MFG protein), E-cadherin (PM), β-actin (cytosol), PdiA3 and GRP78 (ER lumen), calnexin and Stx-18 (ER membrane), and GM130 (Golgi). Note the strong enrichment of PLIN2 in the CLD fraction. BTN1, butyrophilin; E-Cad, E-cadherin; GM130, Golgi matrix protein 130; GRP78, glucose-regulated protein 78; M, whole milk; P1, pellet 1; P2, pellet 2; PdiA3, protein disulfide isomerase A3; PLIN2, perilipin2; S1, supernatant 1; S2, supernatant 2; Stx-18, syntaxin 18; T, total extract.

localization with which they are associated. As shown in Figure 5A (CLDs, function), the identified proteins fell into 13 functional categories. Three major groups of proteins represent ~77% of the total: enzymatic activities (31.01%), protein synthesis, binding and folding (23.64%), and membrane and vesicular trafficking (21.70%). Nearly 72% of the identified proteins were cytoplasmic (Figure 5A, CLDs, cellular localization), whereas the remaining proteins were mainly assigned to the membrane (12.40%), mitochondrion (5.81%), and endoplasmic reticulum (3.49%) categories.

The LC-MS/MS analysis allowed the identification of 395 proteins (peptide FDR = 0.11%) in MFGMs (Supplemental Table S1, MFGM) with an average recovery of ~40% and up to 70% for known major MFG proteins, such as BTN1, fatty acid synthase, XOR, MFG-E8, PLIN2, CIDE-A, cluster of differentiation 36, and mucin1 (Muc1) with previous studies (Wu *et al.*, 2000; Fortunato *et al.*, 2003; Reinhardt and Lippolis, 2006; Affolter *et al.*, 2010; Pisanu *et al.*, 2011; Spertino *et al.*, 2012). Sixty-six (16.71%) of these proteins were associated with ribosomes. As previously mentioned, these ribosomal proteins were excluded for further analysis, and the remaining 329 proteins were classified on the basis of their function (Supplemental Table S1, MFGM function) or cellular localization (Figure 5A, MFGMs; Supplemental Table S1, MFGM localization). A large majority of the identified proteins (~90%) were assigned to the protein synthesis, binding, and folding (27.30%), enzymatic activities (23.62%), membrane and vesicular trafficking (11.35%), immune function (9.20%), fat transport/metabolism (8.28%), and transport (7.36%) categories. About 97% of the identified proteins fell into the following five main cellular localizations: cytoplasm (24.23%), mitochondrion (19.33%), membrane (18.41%), ER (17.48%), and secreted (17.18%). Of note is the striking change in the cellular origin categories of the identified proteins between CLDs and MFGMs (Figure 5A, compare CLDs and MFGMs, right).

Among the proteins associated with either MFGMs (329 proteins) or CLDs (258 proteins), 70 (plus two ribosomal proteins) were found to be common to the two organelles. About 93% of the common proteins (Figure 5A, common) fell into only four functional categories: membrane and vesicular trafficking (21.43%), enzymatic activity (31.43%), protein synthesis, binding and folding (25.71%), and fat transport/metabolism (14.28%). Note that the relative proportions of proteins within the enzymatic activity, protein synthesis, binding and folding, and membrane and vesicular trafficking major function categories were similar in CLDs and among the proteins common to both CLDs and MFGMs, whereas the last category was quite reduced in MFGMs. As to the cellular localization, half of the identified proteins (50.00%) appeared to be cytoplasmic, the remaining common proteins being essentially classified in the categories membrane (21.43%), mitochondrion (11.43%), and endoplasmic reticulum (8.57%).

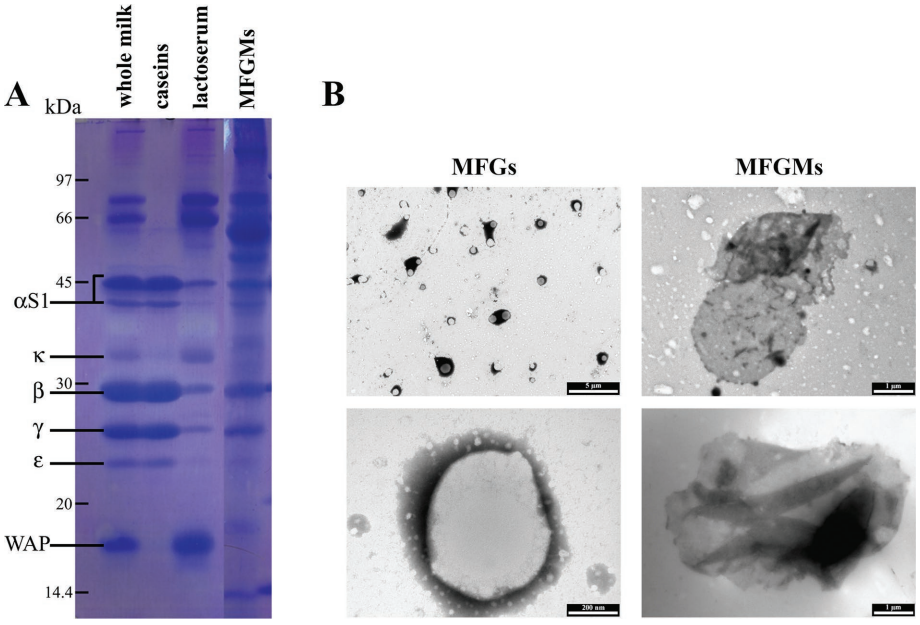

FIGURE 3: Analysis of the different mouse milk fractions and quality of the MFGMs. (A) Whole mouse milk as well as the milk fractions corresponding to caseins, lactoserum, and MFGMs were analyzed by SDS–PAGE on 12.5% acrylamide gel. Caseins appeared to be the main proteins present in mouse milk and were only faintly present in the lactoserum and MFGs fractions. The specific protein pattern observed for MFGMs indicated the minimal contamination by caseins or lactoserum proteins, as well as the enrichment of some proteins in this fraction. Relative molecular masses (kilodaltons) and casein isoforms are indicated on the left. (B) MFGs purified from mouse milk and isolated MFGMs were analyzed by transmission electron microscopy after negative coloration. The MFGs appeared as round structures with a lipid core, whereas MFGMs were devoid of neutral lipid core, cellular debris, or membranous organelles.

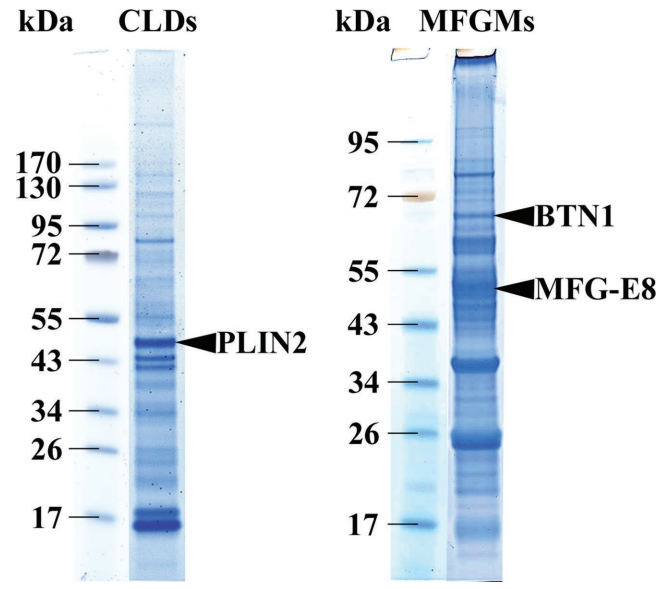

FIGURE 4: Protein profile of the CLDs and MFGMs by 1D SDS–PAGE. CLDs were prepared from mammary acini purified from mouse mammary gland at day 10 of lactation, and MFGMs were recovered from MFGs isolated from mouse milk collected at the same time point, as described in *Materials and Methods*. Proteins (~8 µg) were loaded on 4–12% polyacrylamide gels (NuPAGE Novex, 4–12% Bis-Tris gel, NP002) in MES buffer and further stained with SimplyBlue SafeStain G250 (LC6060; Invitrogen). The relative molecular masses (kilodaltons) are indicated. Marker proteins appeared specifically enriched in each preparation: PLIN2 in CLDs, and BTN1 and MFG-E8 in MFGMs.

The comparison of the functional and cellular localization categories of the proteins identified in CLDs and MFGMs (Figure 5B) clearly shows that the proportion of proteins classified in membrane and vesicular trafficking or cell signaling categories is significantly reduced in MFGs compared with CLDs, whereas that of proteins falling in the immune function and transport categories is significantly increased in MFGMs (Figure 5B, left). On the other hand, the proportion of proteins involved in enzymatic activity, protein synthesis, binding, and folding, and fat transport/metabolism appears quite similar between MFGMs and CLDs. The comparison of the cellular localizations (Figure 5B, right) shows that, whereas the percentage of cytoplasmic proteins is drastically reduced, that of proteins in the ER, mitochondrion, and secreted categories is significantly increased in MFGMs compared with CLDs. Furthermore, the number of ribosomal proteins (excluded from the foregoing analysis) was dramatically increased to 69 proteins in MFGMs, representing up to 17.47% of identified proteins, whereas only 2 ribosomal proteins (0.77%, also found in MFGMs) were found in CLDs (unpublished data).

Taken together, these results suggest that the proteins associated with CLDs and MFGMs greatly differ in terms of functions and cellular origins. The intriguing fact that the proteins assigned to the membrane category were not significantly increased in the secreted MFGs compared with CLDs can be explained by the increase in proteins assigned to the endoplasmic reticulum and mitochondrion groups, as well as in ribosomal proteins. These observations led to the attractive possibility that, in addition to the APM, intracellular compartments such as the ER and mitochondria could provide membrane for the budding of MFGs.

The selective study of membrane-associated proteins favors the involvement of the ER as the source of membrane for MFG budding

To reinforce the hypothesis that membranous intracellular compartments play a role during the budding of MFGs, we analyzed the pool of membrane-associated proteins identified in CLDs and MFGMs in further detail. The number of proteins with single- or multiple-pass transmembrane domains, as well as lipid-anchored proteins, was estimated in both sets of data (Figure 6). This comparison (Figure 6A, left, excluding ribosomal proteins) shows a huge increase in the number of the membrane-associated proteins in MFGMs (96 proteins, 21.36% of the total) compared with CLDs (21 proteins, 8.14% of the total). Of note, this was largely due to the high number of single- and multiple-pass transmembrane proteins in MFGMs. In contrast, the number of lipid-anchored proteins was quite similar in CLDs and MFGMs. Among these proteins, only 13 (61.90% for CLDs and 4.02% for MFGMs) are common to both CLDs and MFGMs, with more than two-thirds (nine) being lipid-anchored proteins. Thus, whereas the number of lipid-anchored proteins appears quite similar in CLDs (15) and MFGMs (17), there is a substantial increase in both

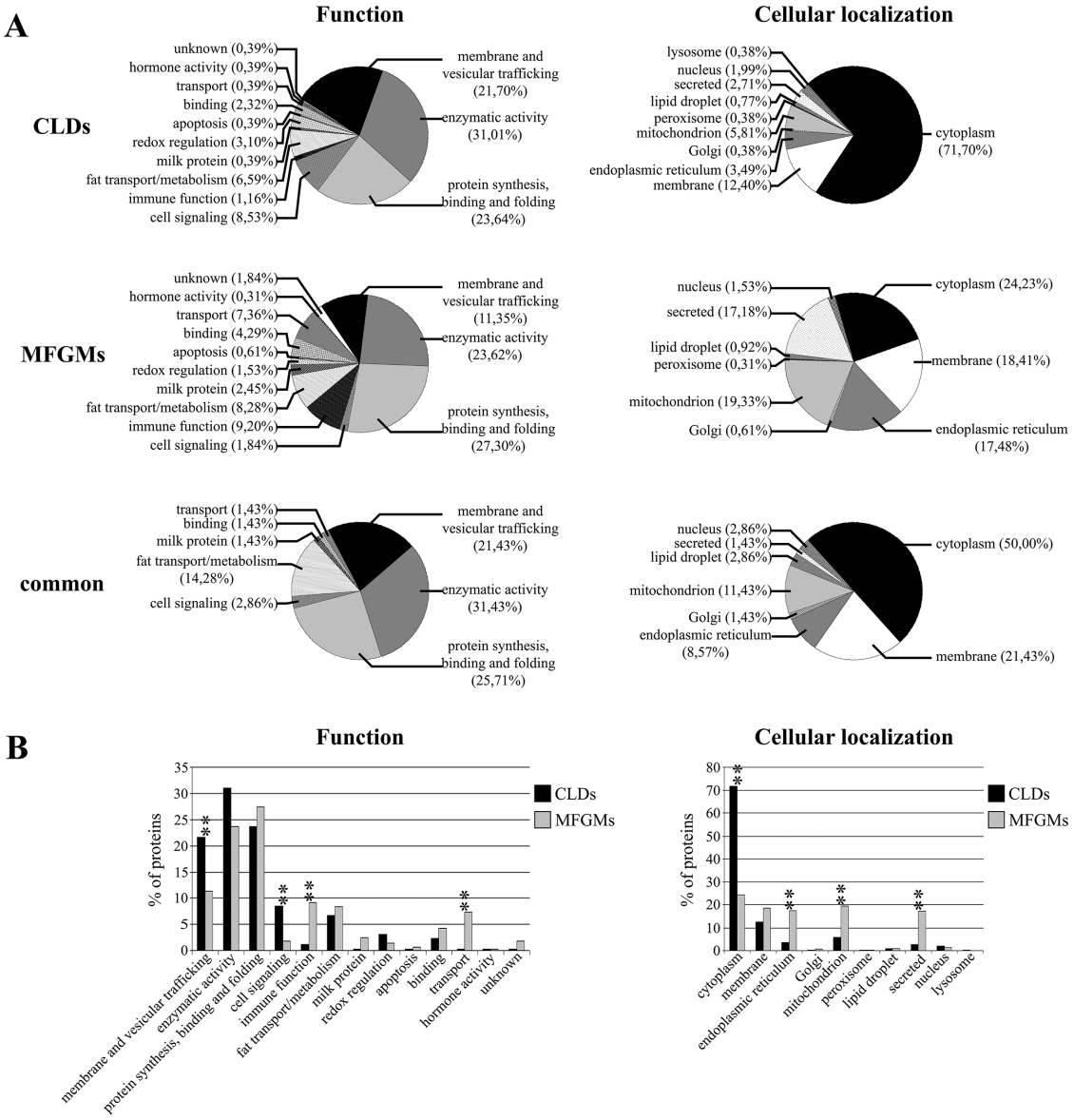

FIGURE 5: Classification of the proteins identified in CLDs or MFGMs based on their biological function or cellular localization. (A) The proteins identified by LC-MS/MS with at least two peptides in CLDs (260 proteins) or MFGMs (395 proteins) were classified by either their biological function (left) or cellular localization (right), according to the GO terms of the Uniprot KB database (Supplemental Table S1). The categorizations of the proteins common to CLDs and MFGMs (72 proteins) are also shown. (B) The relative distributions of the proteins associated with CLDs or MFGMs were compared on the basis of their function (left) or cellular localization (right). Note that the scale of the right graph is twofold greater than that of the left graph. Ribosomal proteins were excluded from these classifications because they would have artificially increased the protein synthesis, binding, and folding functional category, as well as the endoplasmic reticulum cellular localization category. $^{**}p < 0.01$.

single- and multiple-pass transmembrane proteins in MFGMs compared with CLDs. Moreover, when depicted as proportions (Figure 6A, right), our data clearly show that single- and multiple-pass transmembrane proteins are significantly ($p < 0.01$) increased in MFGMs compared with CLDs. Conversely, the proportion of lipid-anchored proteins is reduced in MFGMs compared with CLDs. Of interest, the analysis of the common proteins indicates that the overall ratio of single- and multiple-pass versus lipid-anchored proteins is quite similar to that observed for CLDs but clearly different from the relative distribution obtained for MFGMs.

To gain information on the cellular origins of the membrane-associated proteins identified in CLDs and MFGMs, we classified these proteins on the basis of their cellular localization (Figure 6B). In CLDs (Figure 6B, left), the membrane-associated proteins are mainly assigned to the membrane category (80.95%), whereas those assigned to the endoplasmic reticulum (9.52%), mitochondrion (4.76%), and Golgi (4.76%) categories are clearly underrepresented. In contrast, in MFGMs (Figure 6B, right), membrane-associated proteins assigned to the membrane category still represent 46.88% of proteins, but those in the endoplasmic reticulum and mitochondrion categories represent 35.41 and 11.46% of proteins, respectively. These three cellular localizations account for up to 93.75% of membrane-associated proteins identified in MFGMs.

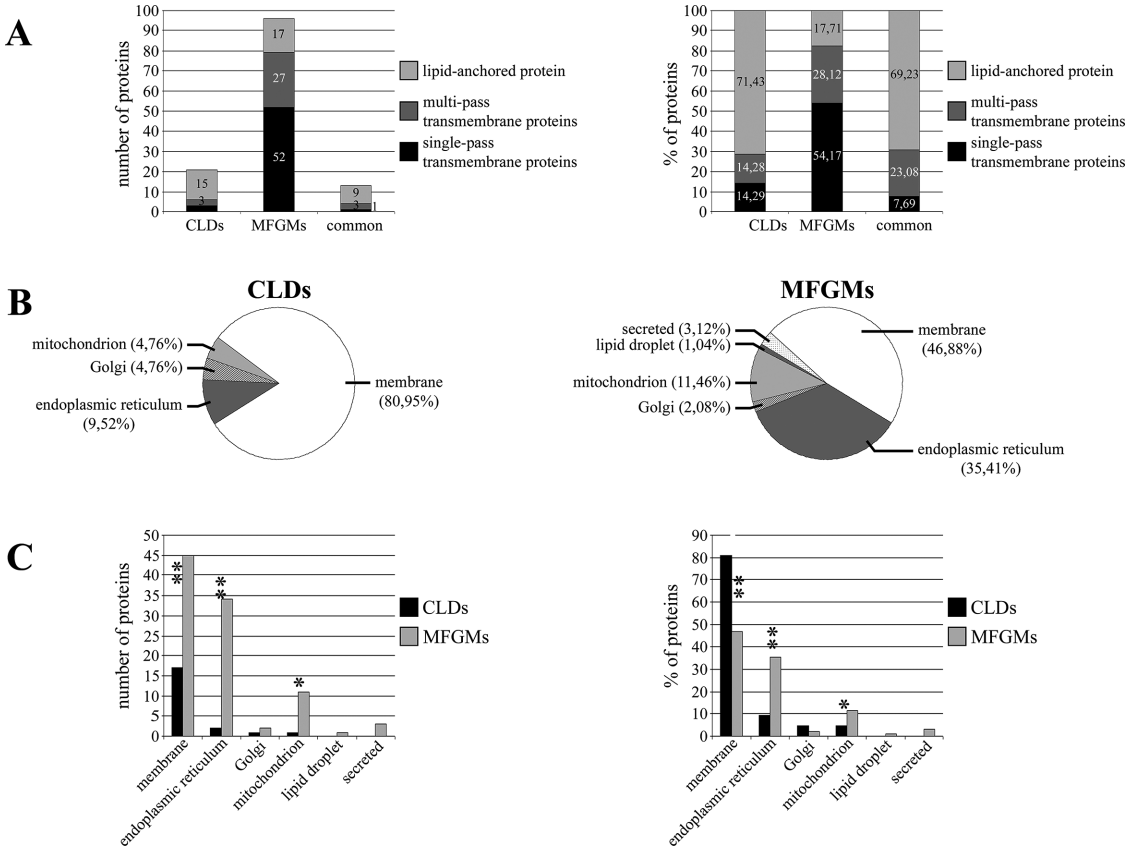

FIGURE 6: Analysis of the membrane-associated proteins identified in CLDs and/or MFGMs. (A) Membrane-associated proteins (single- or multiple-pass transmembrane proteins and lipid-anchored proteins) identified in CLDs, MFGMs, or common to both organelles were specifically analyzed in terms of numbers (left) and percentages (right). (B) Membrane-associated proteins identified in CLDs (left) or MFGMs (right) were classified by their cellular localization. (C) Membrane-associated proteins classified based on their cellular localization were compared between CLDs and MFGMs in terms of number of proteins (left) and proportions (right). *$p < 0.05$; **$p < 0.01$.

The cellular localizations of the membrane-associated proteins were also compared between CLDs and MFGMs, in terms of both numbers (Figure 6C, left) and relative proportions (Figure 6C, right). The results clearly show a significant increase in the number of membrane-associated proteins within the membrane, endoplasmic reticulum, and mitochondrion categories in MFGMs compared with CLDs (Figure 6C, left). However, despite a threefold increase in the number of membrane-associated proteins assigned to the membrane category, their relative proportion significantly decreases (approximately twofold) in MFGMs compared with CLDs, whereas the relative proportion of proteins assigned to the endoplasmic reticulum and mitochondrion categories increases concomitantly with their number (Figure 6C, left vs. right).

As a whole, our analysis shows that, in addition to an increase in the total number of membrane-associated proteins in MFGMs (96) compared with CLDs (21), those identified in MFGMs are mostly transmembrane proteins (82, 29%) whereas those found in CLDs are mainly lipid-anchored proteins (71, 43%). These observations are fully consistent with the membrane topology of these organelles, a phospholipid monolayer for CLDs, and an additional bilayer for MFGs. Moreover, a large majority of membrane-associated proteins present in MFGMs are not found in CLDs. Because membrane-associated proteins can be considered a signature of a given membranous compartment, our results strongly suggest that, besides the APM, the ER and potentially mitochondrion contribute to MFGM formation.

Lipid rafts may be involved in CLD biogenesis and MFG secretion

Because some proteins, such as SNAP23, Muc1, erlin2, prohibitin, and GRP78, were described as being present in lipid rafts (Chamberlain and Gould, 2002; Staubach *et al.*, 2009), we reanalyzed our LC-MS/MS results, focusing on proteins that were already described in raft proteomics studies. Because both the sample preparation and the proteomic method can affect the identification of proteins, we chose four studies based on the facts that 1) they were performed with the same approach used in the present study (1D SDS–PAGE and LC-MS/MS); 2) lipid rafts were extracted using Triton X-100, and 3) they covered different species as well as primary cells and cell lines (human, HeLa cells, Foster *et al.*, 2003; mouse spinal cord, Zhai *et al.*, 2009; NG 108-15 cells [mouse neuroblastoma/rat glioma hybrid], Poston *et al.*, 2011; and rat renal collecting duct cells, Yu *et al.*, 2008). A list of the proteins already found in lipid rafts is given in Supplemental Table S1 (CLD, MFGM, and common raft-associated proteins). This analysis clearly indicates that raft-associated proteins were found in both mouse CLDs and MFGMs (Figure 7A). Surprisingly, these proteins represent a significantly ($p < 0.01$) higher proportion in CLDs (53%) than in MFGMs (38%). Some of these lipid raft–associated proteins were common to both organelles (20.00% in CLDs and 13.16% in MFGMs), whereas others were specifically present in CLD (33.08%) or MFGM (25.32%) preparations, respectively. Moreover, the analysis of the

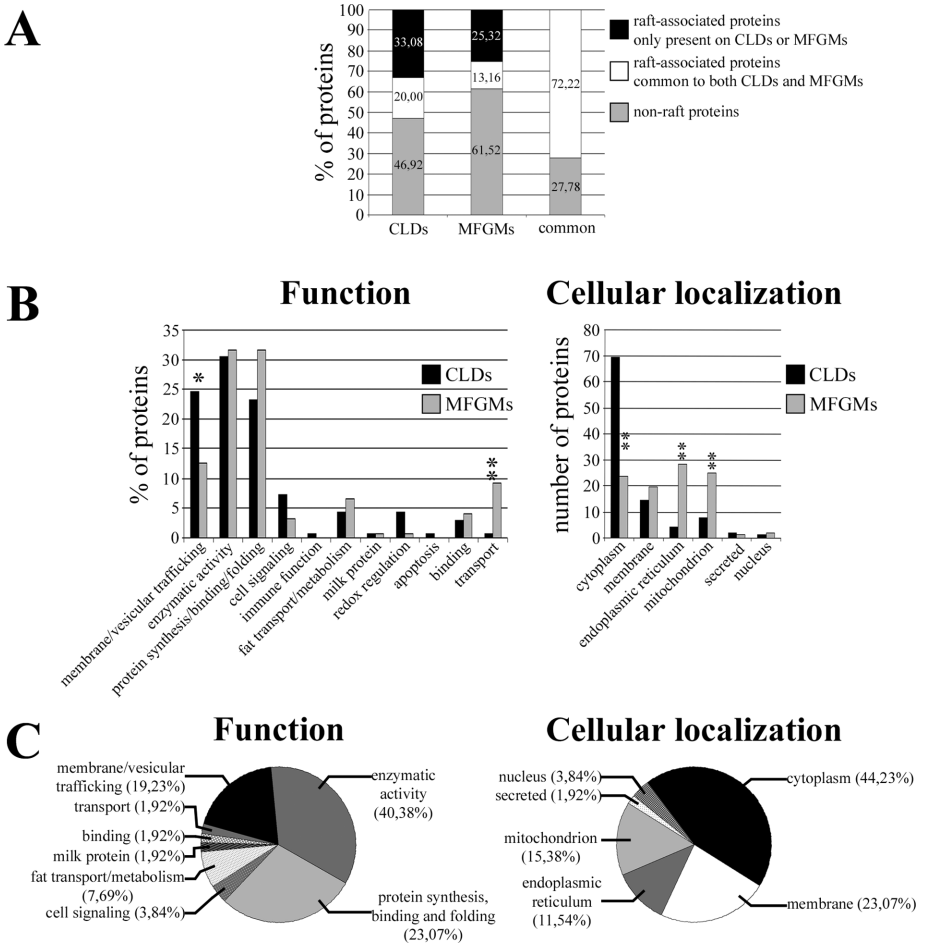

FIGURE 7: Analysis of the proteins associated with lipid rafts in mouse CLDs or MFGMs. Proteins identified by LC-MS/MS in mouse CLDs and MFGMs were classified based on their association with lipid rafts (Supplemental Table S1, CLD, MFGM, and common raft-associated proteins) by comparing them with those already found in lipid rafts in other studies (human HeLa cells, Foster *et al.*, 2003; mouse spinal cord, Zhai *et al.*, 2009; NG 108-15 cells [mouse neuroblastoma/rat glioma hybrid], Poston *et al.*, 2011; rat renal collecting duct cells, Yu *et al.*, 2008; Supplemental Table S1, CLD, MFGM, and common raft-associated proteins). (A) Proteins were classified into three categories: nonraft proteins (gray boxes), lipid raft–associated proteins common to both CLDs (20.00%) and MFGMs (13.16%; white boxes), and raft-associated proteins present only in CLDs (33.08%) or only in MFGMs (25.32%; black boxes). Note that the total of raft-associated proteins is significantly different ($p < 0.01$) between CLDs (53.08%) and MFGMs (38.48%). Data are expressed as percentage of total proteins. (B) The lipid raft-associated proteins identified in CLDs or MFGMs were classified based on their function (left) or cellular localization (right) and compared between the two organelles. *$p < 0.05$; **$p < 0.01$. (C) The lipid raft-associated proteins common to both CLDs and MFGMs were classified based on their function (left) or cellular localization (right).

proteins common to CLDs and MFGMs indicates that only 27.78% are nonraft proteins, whereas the vast majority (72.22%) were found in lipid rafts in at least one of the chosen studies. When the identified raft-associated proteins were classified by function and cellular localization (Figure 7B, left and right, respectively), it clearly appeared that the proteins in the membrane and vesicular trafficking and redox regulation functional categories were significantly decreased, whereas those in the transport category were substantially increased in MFGMs compared with CLDs. The cellular localization cytoplasm category was drastically reduced, whereas the endoplasmic reticulum and mitochondrion categories were significantly increased in MFGMs compared with CLDs. A detailed analysis of the raft-associated proteins common to both CLDs and MFGMs was also performed (Figure 7C). The results indicate that a large majority of these proteins belong mainly to three functional categories (~83%)—enzymatic activity (40.38%), protein synthesis, binding, and folding (23.07%), and membrane and vesicular trafficking (19.23%)—and four cellular localization categories (~94%)—cytoplasm (44.23%), membrane (23.07%), mitochondrion (15.38%), and endoplasmic reticulum (11.54%).

Taken together, these results further support that the ER and potentially mitochondria contribute to the formation of the MFGM and also point to the intriguing possibility that lipid rafts could be linked to the biogenesis of CLDs and/or the secretion of MFGs.

GM1 ganglioside—a lipid raft marker—and cholesterol are associated with both CLDs and MFGs

Because the foregoing results suggest that lipid rafts associate with CLDs and MFGs in MESCs, we studied the subcellular localization of GM1 ganglioside, a known lipid raft marker, by indirect immunofluorescence (IIF) in mouse mammary gland sections at L10 and in purified MFGs (Figure 8). When milk secretion was slowed by separating the pups from the female, GM1 ganglioside appeared to be distributed throughout the MESCs, with a slight association of the labeling with the basolateral PM and some intracellular accumulation frequently surrounding CLDs (Figure 8A, arrows). In the lumen of the acini, GM1 was detected on the surface of budding and secreted MFGs (Figure 8A, arrowheads). The same localizations were observed for GM1 ganglioside in the presence of pups, although its presence in the vicinity of CLDs was less frequent (unpublished data). Because casein-containing SVs are commonly observed around CLDs in the subapical region of MESCs during lactation, GM1 ganglioside and caseins were codetected. As shown in Figure 8B, GM1 ganglioside and caseins both accumulated at the apical side of MESCs when milk secretion was down-regulated, but they were only poorly colocalized (yellow) in discrete areas in MESCs. No intracellular accumulation was observed for caseins, unlike GM1 ganglioside. Moreover, although both GM1 ganglioside and caseins were present on the surface of budding and secreted MFGs, little to no colocalization was observed (Figure 8B, arrowheads). GM1 ganglioside was also detected on the surface of purified MFGs (Figure 8C). The intensity of the GM1 ganglioside labeling was quite variable among the MFGs, and its distribution was heterogeneous on the surface of the MFGs.

Because CH is an obligate component of lipid rafts, it was detected using filipin, a drug known to bind membrane sterols, especially unesterified CH. When milk secretion was slowed, free CH

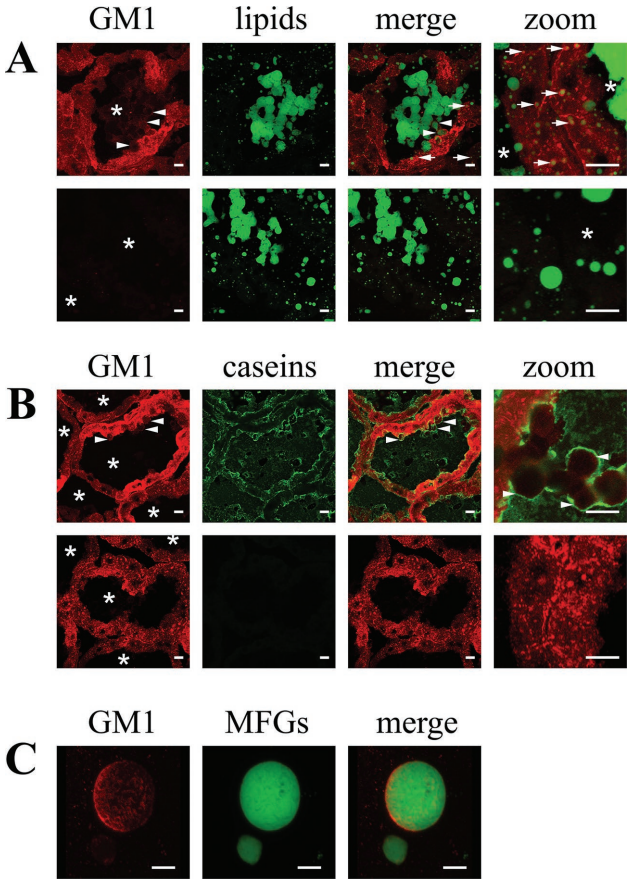

FIGURE 8: GM1 ganglioside, a marker of lipid raft microdomains, is associated with both CLDs and MFGs. The intracellular localization of GM1 ganglioside was studied by fluorescence using Alexa 594–conjugated CTxB in mouse mammary gland at day 10 of lactation in the absence of pups, as well as on MFGs purified from mouse milk collected at the same time point. (A) GM1 ganglioside appeared to be present on the surface of budding and secreted MFGs (arrowheads) and throughout the MESCs, with clear accumulations surrounding the CLDs (arrows). A negative control without CTxB did not show any labeling (bottom). (B) GM1 ganglioside and caseins were codetected in sections of mouse mammary gland at day 10 of lactation. Although both GM1 ganglioside and caseins were associated with budding and secreted MFGs (arrowheads), they only occasionally colocalized. A negative control without primary antibody did not show any labeling or red fluorescence (CTxB). (C) GM1 ganglioside was detected on the surface of MFGs by Alexa 594–conjugated CTxB. All images are *z*- projections (*y*-axis) of confocal stacks. Asterisks indicate lumens. Scale bar, 10 μm (mammary gland sections), 5 μm (MFGs).

was detected throughout the secretory MESCs, with evident accumulation around the CLDs, as well as on the surface of MFGs (Supplemental Figure S2A, arrows and arrowheads, respectively), similar to what was observed for GM1 ganglioside (Figure 8A). Other cell types surrounding the alveolae were also strongly labeled by filipin. Free CH was also present on the surface of permeabilized MFGs (Supplemental Figure S2B). Free CH was found to colocalize with GM1 ganglioside at the basolateral PM of the MESCs, but CH and GM1 ganglioside were only sparsely associated around CLDs and on the surface of MFGs (Supplemental Figure S2C, open arrowheads).

Together with the analysis of raft-associated proteins, the intracellular association of GM1 ganglioside and free CH with CLDs and MFGs suggests an early association of lipid raft components with CLDs and a role of these membrane microdomains in CLD biogenesis and/or MFG secretion.

Intracellular compartment marker proteins are differentially associated with CLDs and MFGMs

To confirm the LC-MS/MS results, we investigated the presence of various proteins in both CLDs and MFGMs by Western blot (Figure 9). We first checked for the presence of two known protein markers of CLDs and MFGMs—PLIN2 and BTN1, respectively. PLIN2 was strongly detected in CLDs and only slightly in MFGMs, whereas BTN1 clearly accumulated in MFGMs compared with CLDs. Two other CLD/MFG markers—Rab18 and XOR—were also identified in both sample types by MS, unambiguously confirming their respective natures. Because MFG budding consumes a huge quantity of membrane, a plausible hypothesis is that the membrane supplied by the exocytosis of SVs is at least partially used to enwrap the MFGs. To further test this possibility, we investigated the presence of the SNAREs involved in milk product trafficking and/or secretion, that is, the Q-SNAREs SNAP23, Stx-3, -4, -6, -7, and -12, and the R-SNAREs VAMP4, VAMP8, and Sec22b (Chat *et al.*, 2011), in CLDs and MFGMs. Of note, LC-MS/MS did not identify SNARE proteins in CLDs, whereas SNAP23, VAMP8, and Sec22b were found in MFGMs. In contrast, Western blot analysis showed that SNAP23 was present in both CLDs and MFGMs, as previously suggested (Liu *et al.*, 2004; Reinhardt and Lippolis, 2006; Bostrom *et al.*, 2007; Affolter *et al.*, 2010). Other Q-SNAREs (Stx-3, -4, -6, -7, and -12) were all detected in MFGMs, but only Stx-6 and -12 were also found in CLDs. A surprising result was the clear accumulation of Stx-4 in MFGs compared with CLDs, as this SNARE was previously localized to the basolateral PM of lactating MESCs (Chat *et al.*, 2011). As for the R-SNAREs, VAMP4 was detected in both CLDs and MFGMs, whereas VAMP8 and Sec22b were present only in MFGMs. Note that, for VAMP4, a doublet was observed in MFGMs, suggesting a possible change in the phosphorylation status and/or the presence of VAMP4 variants associated with MFGMs compared with CLDs. Because our previous work suggested that, at the least, SNAP23 and VAMP8 were most likely involved in the exocytosis of caseins, the present results suggest that the membrane delivered at the APM of lactating MESCs after fusion of casein-containing SVs is reused to enwrap the budding MFGs. Moreover, together with the detection of three ER-resident proteins—calnexin, GRP78, and PDIA3, which were also identified by LC-MS/MS—the presence of Sec22b in MFGMs but not in CLDs supports a strong interaction between the ER and CLDs and the possibility that the ER contributes to the formation of the MFGM, as Sec22b is an ER-resident transmembrane SNARE.

The presence of other proteins identified by MS in both CLDs and MFGMs (Rab7A GTPase) or only in CLDs (AnxA2) or not found in our study but shown to be associated with CLDs in other cell types (caveolin1 [Cav1]) was also investigated. Rab7A appeared to be enriched in MFGMs compared with CLDs, whereas Cav1 and AnxA2 were only detected in CLDs. These observations suggest that, whereas certain proteins are specifically associated with the secreted MFGs, others, such as Cav1 and AnxA2, are likely sorted away from the budding MFGs to be retained in the cell. In addition, erlin2 and flotillin2, two known protein markers of lipid rafts, were clearly detected in MFGMs but not in CLDs.

Taken together, our Western blot results suggest that some SNARE proteins are associated with CLDs (SNAP23, Stx-6 and -12, VAMP4), whereas others are present only in MFGMs (Stx-3, -4, and -7, VAMP8, and Sec22b). The appearance of Stx-7, Stx-12, and

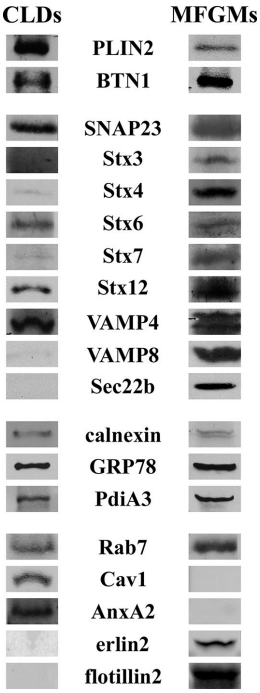

FIGURE 9: Western blot analysis of a number of proteins associated with mouse CLDs and/or MFGs. The presence of some of the proteins identified in CLDs and/or MFGs by LC-MS/MS was investigated by WB. CLDs were isolated by flotation on a sucrose gradient from acini purified from murine mammary gland at day 10 of lactation. MFGs were isolated from mouse milk collected at the same time point, and MFGMs were extracted. The following types of proteins were analyzed: protein markers of CLDs (PLIN2) and MFGs (BTN1), SNARE proteins (SNAP23, syntaxins 3, 4, 6, 7, and 12, VAMP4, VAMP8, and Sec22b), ER-resident proteins (calnexin, GRP-78, and PDIA3), other proteins related to membrane trafficking (Rab7, Cav-1, and AnxA2), and raft microdomain markers (erlin2 and flotillin2). AnxA2, annexin A2; BTN1, butyrophilin; Cav-1: caveolin-1; GRP78, glucose-regulated protein 78; PDIA3, protein disulfide isomerase A3; PLIN2; adipophilin; SNAP23, synaptosomal-associated protein of 23 kDa; Stx, syntaxin; VAMP, vesicle-associated membrane protein.

VAMP8 in MFGMs strongly supports the possibility that, after exocytosis, the membrane from casein-containing SVs is incorporated into the MFGM. Furthermore, the clear emergence of erlin2 and of the ER-resident SNARE Sec22b is consistent with the contribution of the ER to the MFGM. In addition, the presence of erlin2 and flotillin2 in MFGM but not in CLDs argues for a role of lipid rafts in MFG secretion.

The spatiotemporal association of some proteins with CLDs and MFGs depends on the secretory activity of MESCs

To obtain further information on certain proteins associated with CLDs and/or MFGMs, we localized Muc1, PLIN2, BTN1, and Rab18 and 7 at the subcellular level by IIF in mouse mammary tissue sections at L10 (Figure 10). Because SNARE proteins and Rab GTPases cycle between donor and acceptor compartments, we performed analyses under experimental conditions that slow milk secretion (Wilde *et al.*, 1999; Weaver and Hernandez, 2016). In these conditions, the high membrane turnover required for milk product transport and secretion is limited, and cycling proteins preferentially reside in their compartment of origin. Moreover, the observation of the APM of MESCs is also facilitated because the lumen of the acini is dilated by the accumulation of milk products. The pups were either left with the female (Figure 10, +p) or, to slow milk secretion, separated from the female for 4 h (Figure 10, –p) before the mammary gland was removed. Muc1 and BTN1, two MFG protein markers, were both mainly accumulated at the apical side of lactating MESCs (Figure 10, Muc1 and BTN1). Muc1 labeling was exclusively associated with the APM of lactating MESCs. Note the important morphological change in MESCs, mainly at their apical side, upon suckling (Figure 10, Muc1, compare +p and –p). Muc1 was also observed on secreted MFGs present in the lumen of the acini (Figure 10, Muc1, arrowheads) but did not appear to be associated with CLDs, even when in the vicinity of the APM (Figure 10, Muc1, zoom). As expected, BTN1 was mainly localized to the APM of the lactating MESCs, as well as on the surface of the budding and secreted MFGs (Figure 10, BTN1, arrowheads). However, unlike Muc1, BTN1 was also occasionally observed surrounding the CLDs localized beneath the APM of MESCs (Figure 10, BTN1, arrows). PLIN2, a CLD protein marker, labeled most of the CLDs (Figure 10, PLIN2), which appeared to have chiefly accumulated in the subapical region of MESCs under conditions slowing the secretion of milk products (Figure 10, PLIN2, –p, arrows). PLIN2 was also observed around budding and secreted MFGs in the lumen of the acini (Figure 10, PLIN2, arrowheads). As for Rab18, it was distributed throughout the cells, with a clear accumulation at the basal side of MESCs, around CLDs (Figure 10, Rab18, +p, arrows), and at the surface of both budding and secreted MFGs (Figure 10, Rab18, +p, arrowheads). However, when secretion was slowed, Rab18 labeling was more prominent around CLDs, which accumulated in the subapical region of MESCs (Figure 10, Rab18, –p, arrows), whereas the basal side was no longer labeled. Finally, we investigated the localization of Rab7, which was identified in both CLDs and MFGMs by MS (Figure 10, Rab7). During suckling, Rab7 labeling appeared to be distributed throughout the cytoplasm, with clear accumulation around some CLDs (Figure 10, Rab7, +p, arrows), and in the vicinity of the PM of MESCs. Rab7 was also faintly detected at the surface of secreted MFGs (Figure 10, Rab7, +p, arrowheads). When secretion was slowed, Rab7 seemed to be less cytoplasmic and more tightly accumulated beneath the PM, particularly at the apical side of the MESCs. Similarly, the accumulation of Rab7 around CLDs was less frequently observed (Figure 10, Rab7, –p). Negative controls with no primary antibody did not show any labeling (Figure 10, –Ig1).

Taken together, these results suggest that the proteins studied here are associated with CLDs and/or budding MFGs with different spatiotemporal kinetics, depending on the secretory activity of MESCs.

PLIN2 and BTN1 are both associated with apical CLDs and colocalize on the surface of MFGs during suckling

Although the molecular mechanisms involved in the budding of MFGs are not fully understood, one view is that the PLIN2 present on the CLDs may associate, even transiently, with the BTN1 localized at the APM, forming a tripartite complex with XOR, a cytoplasmic protein, to zip the membrane around the budding MFGs. If so, at least PLIN2 and BTN1 should be colocalized at the surface of the budding and secreted MFGs. As expected, PLIN2 was mostly associated with CLDs (Figure 11, PLIN2, arrows), whereas the bulk of BTN1 was localized to the APM of MESCs (Figure 11, BTN1) and sometimes around apical CLDs (Supplemental Movie S1). When secretion was slowed, PLIN2 appeared to be localized around CLDs (Figure 11, –p, PLIN2, arrows), which mostly accumulated at the apical side of MESCs. Although PLIN2 and BTN1 were both present in the subapical region of MESCs, they appeared only

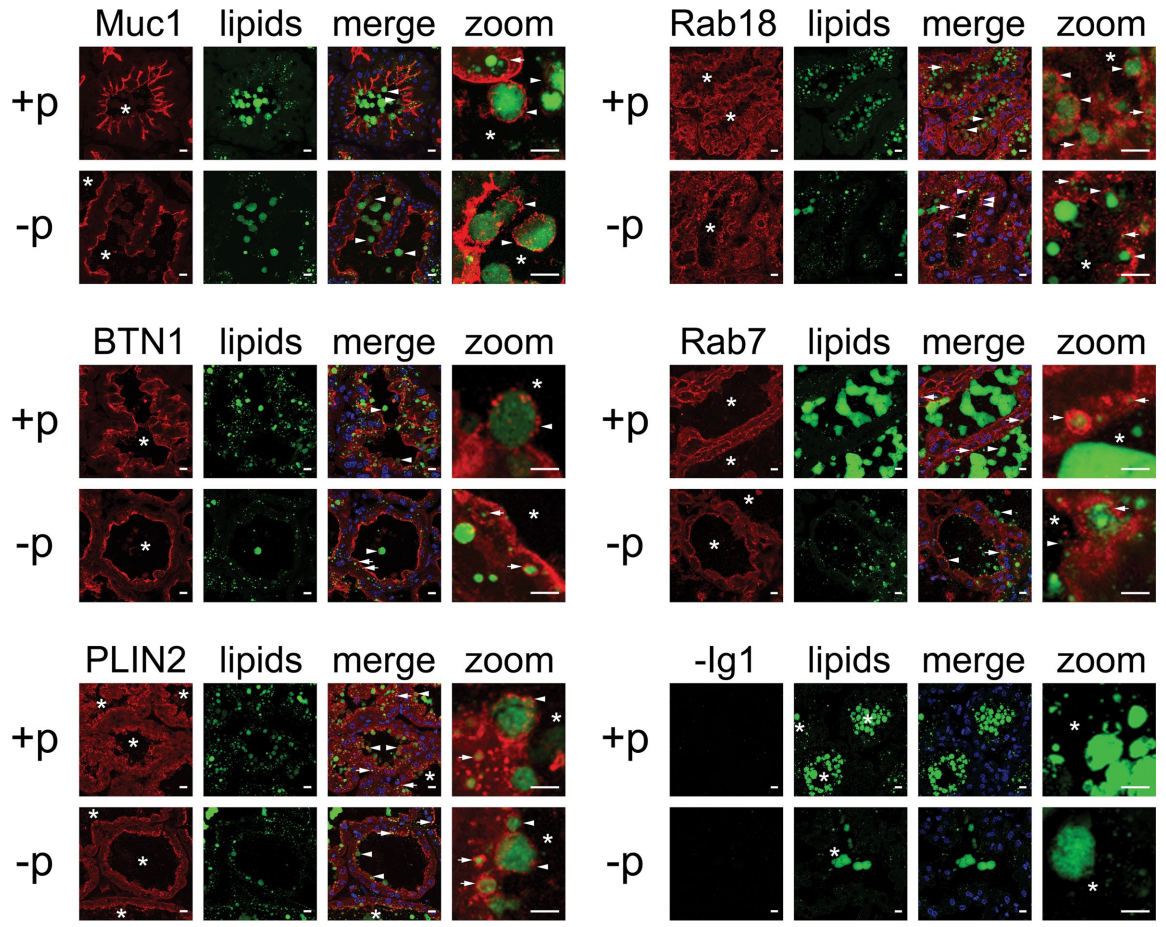

FIGURE 10: Cellular localization of proteins identified in CLDs and/or MFGs in the mouse mammary gland during lactation. The intracellular localization of different proteins associated with CLDs and/or MFGMs was studied by IIF on mouse mammary gland at day 10 of lactation in the presence (+p) or absence of pups (–p). The indicated proteins are in red; neutral lipids (CLDs and MFGs) are in green; DNA was stained with DAPI (blue); the merge shows the superposition of the colored images. Mucin-1 (Muc1) and butyrophilin (BTN1) were essentially localized at the APM of MESCs and around budding and secreted MFGs in the lumen of acini (arrowheads). BTN1 was also observed surrounding apical CLDs (arrows) in the absence of pups. Adipophilin (PLIN2), as well as the small GTPases Rab18 and Rab7, were observed around both CLDs (arrows) and MFGs (arrowheads). Note that these latter markers also appeared to accumulate in the subapical region of MESCs in the absence of pups. All images are *z*-projections (*y*-axis) of confocal stacks. Asterisks indicate lumens. Scale bar, 10 μm.

sparsely colocalized (Figure 11, –p, merge 1, open arrowheads, and Supplemental Movie S2). Conversely, they were clearly colocalized on the surface of secreted MFGs (Figure 11, –p, merge 1, arrowheads). Of interest, the colocalization of PLIN2 and BTN1 appeared to be enhanced (Figure 11, +p) upon suckling, notably on the surface of budding and secreted MFGs (Figure 11, PLIN2 and BTN1, +p, arrowheads, and Supplemental Movie S3). Moreover, PLIN2 and BTN1 also occasionally colocalized around CLDs present just beneath the APM (Figure 11, –p, +p, merge 1, open arrowheads), suggesting that a pool of BTN1 could associate with CLDs before they reach the APM of MESCs (Supplemental Movie S1). Negative controls without primary antibodies (Figure 11, –Ig1) did not show any labeling.

These observations indicate that PLIN2 and BTN1 are in close proximity only on the surface of both budding and secreted MFGs, suggesting that their association, even if transient, mostly occurs on the apical side of MESCs, probably to tightly wrap the APM around the budding MFGs at the time of suckling.

Protein markers exhibit different distributions on the surface of MFGs

To observe directly the distribution of some of the proteins identified by MS, we performed IIF on purified MFGs. Because the gelatin used to embed the MFGs generated some fluorescence background, we systematically imaged the MFGs that were trapped in the air bubbles of the preparation. Note that 1) MFGs were fixed before being embedded in gelatin, as there appeared to be no difference in the distribution pattern of the studied proteins compared with nonfixed MFGs (unpublished data), and 2) for all the IIF experiments, MFGs were permeabilized with saponin 0.05% in phosphate-buffered saline (PBS) in order not to extract CH from the putative lipid rafts within the MFGM. Because the polymeric immunoglobulin receptor (pIgR) has been shown to be present on MFGs, we first performed IIF experiments with irrelevant primary antibodies in order to ensure that any labeling observed was not due to unspecific capture of the antibodies by this receptor. Two antibodies were used for this control experiment: a mouse monoclonal antibody

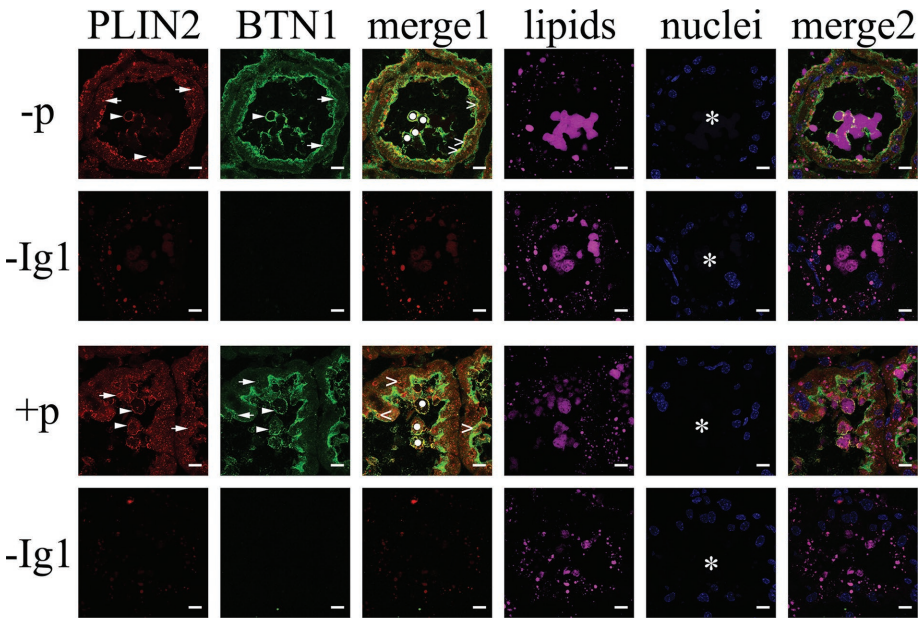

FIGURE 11: Codetection of PLIN2 and BTN1 in mouse mammary gland at day 10 of lactation by IIF. The intracellular localization of two protein markers associated with CLDs and/or MFGs was studied by IIF on tissue sections from the mammary gland of mice in the absence (–p) or presence of the pups (+p) at day 10 of lactation. Neutral lipids were stained with BODIPY 493/503 (magenta false color), and DNA was stained with DAPI (blue). PLIN2 (red false color) was observed throughout the MESCs, with clear accumulations around CLDs (arrows) and on the surface of MFGs (arrowheads). BTN1 (green) was quite exclusively localized at the apical side of MESCs, with some light but visible labeling around apical CLDs (arrows), as well as around MFGs (arrowheads). No clear colocalization of PLIN2 and BTN1 was observed in the apical region of MESCs, with the exception of apical CLDs (merge 1, open arrowheads) and MFGs (merge 1, white circles). Note that the colocalization between PLIN2 and CLD seems to be increased on the surface of MFGs upon suckling (merge 1, white circles; compare –p and +p). Merge 2 shows the four-color picture resulting from the superposition of previous ones. Negative controls without primary antibodies (–Ig1) did not show any labeling. All images are *z*-projections (*y*-axis) of confocal stacks. Asterisks indicate lumens. Scale bar, 10 µm.

(homologous interaction with the pIgR) directed against C23/nucleolin, a nuclear protein; and a rabbit polyclonal antibody (heterologous interaction with the pIgR) against ARK2/Aurora. As shown in Supplemental Figure S3, no labeling was observed for either of these antibodies or with secondary antibodies alone. PLIN2 and BTN1, two known protein markers of CLDs and MFGs, respectively, both displayed a discrete and punctate distribution on the surface of MFGs (Figure 12, BTN1, PLIN2). MFGs appeared heavily stained for Rab18, another CLD/MFG protein marker (Figure 12, Rab18). Rab7, which was identified in both CLD and MFG samples by MS, was also clearly detected on the surface of MFGs (Figure 12, Rab7). Finally, SNAP23 (Figure 12, SNAP23, and Supplemental Movie S4) and VAMP8 (Figure 12, VAMP8, and Supplemental Movie S5), two SNARE proteins involved in casein exocytosis, were clearly detected on the surface of MFGs as numerous and intense small patches. Of interest, SNAP23 and VAMP8 were not detected when the permeabilization step was omitted, and the labeling corresponding to SNAP23 was markedly decreased when Triton X-100 0.2% was used instead of saponin 0.05% (unpublished data). These observations were in agreement with 1) the localization of the SNARE proteins inside the MFGM, which is consistent with the formation of a SNARE complex on the cytoplasmic side of the APM for casein exocytosis, and 2) the fact that SNAP23 is found within "Triton-sensitive" membranes and/or extracted by this detergent due to its palmitoyl membrane anchor (Chamberlain and Gould, 2002; Puri and Roche, 2006). Because SNAP23 and VAMP8 have been described as being localized in lipid rafts, we also attempted to colocalize these proteins with GM1 ganglioside (Figure 8C). However, for unknown reasons, convincing results were not achieved whatever the procedure used (GM1 first/SNARE second or SNARE first/GM1 second), the intensity of both labelings being low (unpublished data). As expected, Muc1, which is localized on the extracellular leaflet of the APM of MESCs (Figure 10, Muc1), was detected on the surface of the MFGs even when the permeabilization step was omitted (unpublished data). Negative controls without primary antibody showed no labeling (Figure 12, –Ig1).

Taken together, these results show that various proteins previously identified by LC-MS/MS in MFGMs all display a punctate distribution pattern on the surface of MFGs, with some differences in the density and homogeneity of the observed labeling. The presence of SNAP23 and VAMP8 inside the MFGM strongly argues for the membrane supplied by casein exocytosis being reused for the budding of MFGs.

DISCUSSION

During lactation, MESCs produce and secrete large amounts of milk from their apical side. Milk proteins, transported along the secretory pathway, are released by exocytosis, whereas MFGs are expulsed by budding, enwrapped by the APM bilayer. Thus, at the time of suckling, there is both membrane supply and loss at the APM of MESCs due to SV fusion and MFG budding, respectively. Moreover, because of the high number and the large size of MFGs (several micrometers in diameter), the amount of membrane needed for their secretion may exceed the APM surface available. We hypothesized that differential analysis of the protein profiles of CLDs and secreted MGFs would lead to the identification of molecular actors and membranous organelles involved in MFG secretion. After validation of the methods used to prepare CLDs and MFGMs, we analyzed the samples by LC-MS/MS and obtained protein profiles consistent with those published for mouse (Wu *et al.*, 2000) and other (Fortunato *et al.*, 2003; Reinhardt and Lippolis, 2006; Pisanu *et al.*, 2011) species and cell types (Liu *et al.*, 2004; Turro *et al.*, 2006; Wan *et al.*, 2007). Indeed, 260 proteins were identified in CLDs and 395 in MFGMs, but, surprisingly, only 72 were found to be common to both. Of note, cytoplasmic crescents containing various intracellular organelles have been described between the lipid core and the outer membrane of the MFGs in all species (Wooding and Peaker, 1970; Patton and Huston, 1988). However, we assume that these structures are unlikely to contribute significantly to the presence of intracellular proteins found in MFGMs because 1) the incidence of these structures is low and depends on the species, 2) mouse MFGs contain very little cytoplasm (Wu *et al.*, 2000), and 3) cytoplasmic crescents, the incidence of which was <3% in mouse MFGs (Supplemental Figure S1), were not observed in our MFGM preparations (Figure 3). When classified based on their function, proteins found in CLDs are mostly involved

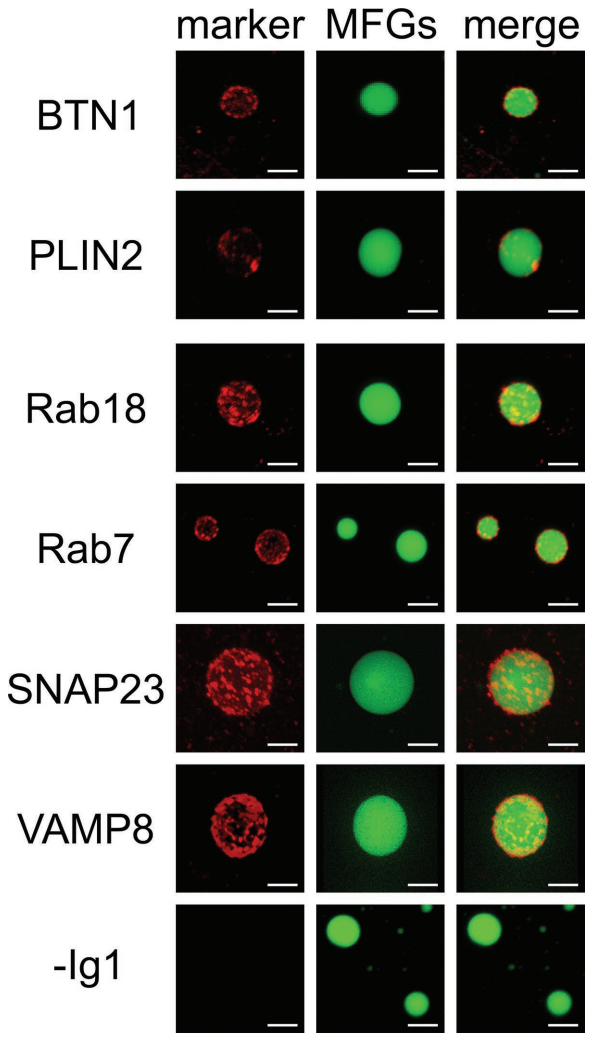

FIGURE 12: Distribution of BTN1, PLIN2, Rab18 and 7 GTPases, and SNAP23 and VAMP8 SNARE proteins on mouse MFGs. Mouse milk was centrifuged, and MFGs present in the cream fraction were embedded in PBS/20% gelatin and immediately frozen. Cryosections (5 µm) were incubated with the indicated antibodies and processed for IIF. A punctate, more or less dense and homogeneous labeling was observed at the surface of the MFGs for all markers studied (red). Neutral lipids were labeled with BODIPY 493/503 (green). All images are *z*-projections (*y*-axis) of confocal stacks. Scale bar, 5 µm.

in the metabolism, synthesis, and binding and folding of proteins or membrane and vesicular trafficking. In MFGMs, the membrane and vesicular trafficking and cell signaling functions are reduced, whereas the immune function and transport categories are increased, compared with CLDs. These variations probably reflect the transition between CLDs, which are dynamic crossroads for glucide, proteic amino acid, and fat metabolism, and MFGs, which are mainly intended to feed and immunologically protect the newborn. Of interest, the classification of the identified proteins based on their cellular localization shows a striking change between CLDs and MFGMs. Whereas cytoplasmic proteins account for >70% of the proteins identified in CLDs, they only represent ~24% of the proteins identified in MFGMs, with a concomitant increase of the membrane, endoplasmic reticulum, mitochondrion, and secreted categories up to ~18% each. Furthermore, a limited number (21) of membrane-associated proteins, which are mostly lipid anchored (71%), are found on CLDs, whereas single- and multiple-pass transmembrane proteins account for up to 82% of the 96 membrane-associated proteins identified in MFGMs. In addition, although the number of lipid-anchored proteins is quite similar in CLDs (15) and MFGMs (17), they represent only ~18% of membrane-associated proteins in MFGMs (four times less than in CLDs) due to the huge increase in the number of transmembrane proteins in MFGMs compared with CLDs. This drastic change reflects the fact that CLDs are surrounded by a phospholipid monolayer containing mainly lipid-anchored proteins, whereas MFGs are surrounded by an additional bilayer arising from various cellular compartments.

CLDs are believed to form by accumulation of neutral lipids within specific domains of the ER called mitochondria-associated ER membranes (MAMs; Rusinol *et al.*, 1994; Stone *et al.*, 2009). Ultrastructural studies have shown that the ER is tightly wrapped around CLDs (Blanchette-Mackie *et al.*, 1995), with ribosome-rich contact points (Ozeki *et al.*, 2005). This connection makes sense, as the enzymes catalyzing the final steps of neutral lipid synthesis reside in the ER. Proteins with no obvious link to CLD functions are also commonly found in CLD preparations, reflecting the physical and functional interactions of CLDs with other membranous organelles (Barbosa *et al.*, 2015; Gao and Goodman, 2015). These interactions have been shown to be regulated by a narrow number of Rab GTPases (Kiss and Nilsson, 2014) and sometimes involve SNARE proteins (Jagerstrom *et al.*, 2009).

Several mechanisms probably underlie the maintenance of the APM surface. Although de novo membrane synthesis cannot totally be ruled out, other nonexclusive sources of membrane seem to be involved in the building of the MFGM. First, a substantial portion of the MFGM obviously comes from the APM of the cell, the deployment of microvillosities providing both a large membrane surface and a favorable context for secretion due to a local reduction of the surface tension. Other mechanisms, including membrane insertion after SV exocytosis (Dai and Sheetz, 1995) and cortical cytoskeleton rearrangement, also locally decrease membrane tension (Raucher and Sheetz, 2000). Second, the membrane supplied by the fusion of many SVs with the APM can also be used to enwrap the MFG (Wooding and Sargeant, 2015; present study). Indeed, the presence in MFGMs of some SNARE proteins (SNAP23, VAMP8, Stx-7, and Stx-12), which have been localized on the surface of SVs (Chat *et al.*, 2011), supports this possibility. Moreover, this would have the double advantage of allowing the release of milk components and of balancing, at least in part, the membrane loss caused by MFG release. As suggested on the basis of a limited number of proteins (Wu *et al.*, 2000), our results strongly support a third possibility: that, in addition to the APM, some intracellular compartments, such as the ER, significantly contribute to MFGM formation. Intriguingly, the ER has already been involved in other "membrane-consuming processes," such as phagocytosis (Desjardins, 2003), when the PM must rapidly expand around the engulfed particles. In this case, the ER provides up to 20% of the early phagosome membrane together with endomembranes of various origins (i.e., PM, endosomes, and lysosomes; Garin *et al.*, 2001; Campbell-Valois *et al.*, 2012). In this case, only a subset of ER proteins is recruited to the early phagosome, suggesting that specific subdomains of this organelle might be involved in phagocytosis. Moreover, two ER-resident SNAREs, Sec22b and Stx-18, have been implicated in ER–PM/phagosome fusion (Hatsuzawa *et al.*, 2006; Cebrian *et al.*, 2011), and SNAP23, as well as Stx-7 and Stx-12/13, regulates phagosome formation and maturation (Collins *et al.*, 2002; Sakurai *et al.*, 2012). The physiological significance of connecting cellular membranes has been described in eukaryotic cells (reviewed in Prinz, 2014; Schrader *et al.*, 2015; Phillips and Voeltz, 2016). Indeed,

the ER has been demonstrated to interact with the PM, allowing bidirectional regulated transfer of lipids, small molecules, and ions without membrane fusion. Of interest, the translocon of the rough endoplasmic reticulum (RER) was shown to interact directly with the PM-bound exocyst (Guo and Novick, 2004), and the ER protein VAMP-associated protein (VAP; also found in MFGMs in this study) forms bridging complexes with peripheral membrane proteins on the PM, as well as other sites in the cell (Loewen *et al.*, 2003). Because ER displays a nonuniform compartmentalization in structurally and functionally specialized regions (reviewed in Borgese *et al.*, 2006; Friedman and Voeltz, 2011; Westrate *et al.*, 2015), our results also suggest that MFGMs at the least contain RER due to the high number of ribosomal proteins and factors involved in translation, and also transitional ER, based on the identification of several ER exit site–resident proteins (five COP subunits, Rab1, Mia3, transmembrane emp24-like trafficking proteins 2, 3, 5, and 10, and valosin-containing protein). Unexpectedly, our results also suggest that a fraction of the MFGM could arise, although to a lesser extent, from the mitochondrial membrane (63 proteins, of which 11 [17.46%] are transmembrane proteins). Mitochondria and ER are functionally related and physically linked through MAMs, explaining how some integral proteins, such as the voltage-dependent anion channel ("porin"), are shared by both organelles (Shoshan-Barmatz *et al.*, 2004).

Lipid rafts play a role in membrane trafficking, particularly in exocytosis and membrane-consuming processes such as phagocytosis (Goyette *et al.*, 2012) and membrane resealing (Miller *et al.*, 2015). Of interest, some proteins classically found in these microdomains (caveolin, prohibitin, Muc1, SNAP23, nicastrin, and erlin2) were identified in CLDs and/or MFGMs. Furthermore, the accumulation of GM1 ganglioside (Figure 8) and free CH (Supplemental Figure S2) around CLDs and MFGs is consistent with previous observations in adipocytes (Prattes *et al.*, 2000) and the presence of lipid rafts on MFGM (Lopez and Menard, 2011). Thus our results indicate that, in lactating MESCs, lipid rafts associate early with the CLDs and could play a role in their biogenesis and/or secretion.

Thus a possible model emerges (Figure 13) in which SNAREs could be central actors to coordinate membrane supply and loss and promote the synchronized secretion of milk products during suckling. Indeed, whereas BTN1, PLIN2, and XOR likely contribute to the MFG budding (Figure 13, 1), SNARE proteins could connect the surrounding SVs not only together, but also with the budding MFGs and the APM through the formation of SNARE complexes (Figure 13, asterisks; Chat *et al.*, 2011). In this way, SNARE proteins could promote both the exocytosis of caseins (Figure 13, 2) and the connection of the ER with the APM to provide membrane to enwrap the budding MFG (Figure 13, 3). In this case, the final step of MFG release likely occurs upon homotypic fusion of the SVs surrounding the budding MFG (Figure 13, 4; apocrine secretion) rather than by final scission of the PM at a budding neck (Wooding, 1971; Kralj and Pipan, 1992). This model would have the double advantage of allowing release of milk components and, at least in part, balancing membrane loss caused by MFGs release. This scenario supports a central regulatory role for SNARE proteins in spatiotemporally coordinated membrane exchanges underlying synchronized secretion of milk products (Truchet *et al.*, 2014).

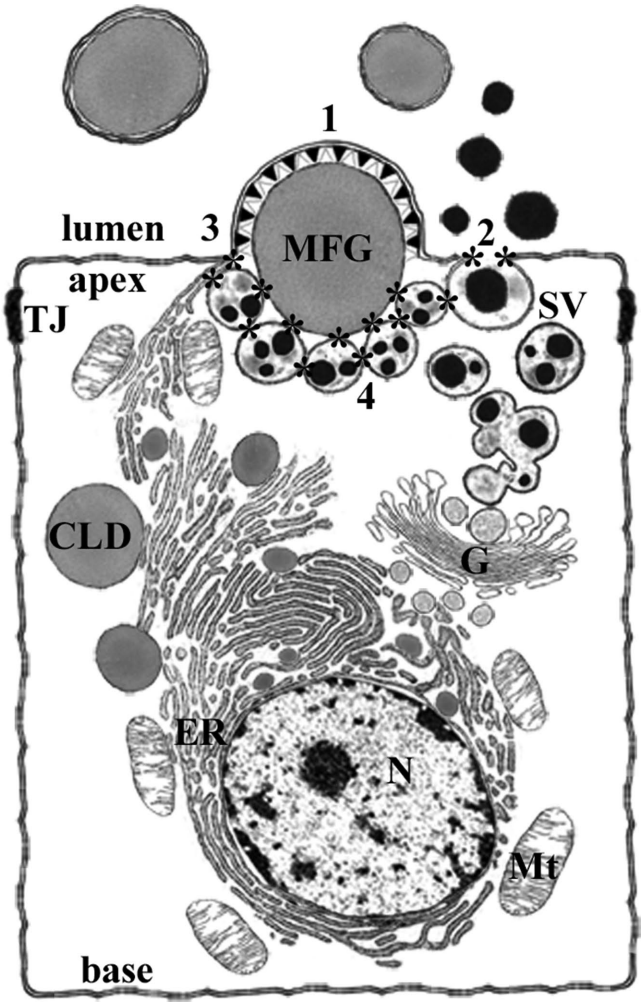

FIGURE 13: Model illustrating the coordinated secretion of milk products in MESCs. CLDs grow by accumulation of neutral lipids between the two leaflets of the ER, and are released by budding (1) as MFGs at the apical side of the MESCs. Caseins, the major milk proteins, are synthesized within the ER, transported along the secretory pathway, and released by exocytosis (2) upon the formation of SNARE complexes (asterisks) containing SNAP23 and VAMP8. Given that these two SNARE proteins were 1) observed at the interface between budding MFGs and casein-containing SVs in the subapical region of lactating MESCs (Chat *et al.*, 2011), and 2) found to be present on MFGs (present study), the membrane provided by exocytosis of the SVs is likely reused to enwrap the MFG during its budding. Moreover, our results strongly suggest that MFGM also arises from intracellular membranous compartments such as the ER and potentially mitochondria. The direct or indirect connection between the ER and the APM (3) explains the presence of Sec22b in the MFGM. Together with xanthine oxidoreductase, the CLD-associated protein PLIN2 (white triangles) and the MFG marker BTN1 (black triangles) may interact to zip the APM at the surface of the MFG during its budding. The accumulation of some protein markers, including some SNAREs, at the base of budding MFGs suggests a possible homotypic fusion of SVs (4) in this area. This would favor both secretion of casein micelles and release of MFGs in the lumen of the alveoli by providing additional membranes for the budding process. G, Golgi apparatus; Mt, mitochondrion; N, nucleus; TJ, tight junction.

MATERIALS AND METHODS

Animals

CD1 mice were bred at INRA (UE0907 IERP, Jouy-en-Josas, France). After parturition, the number of pups per mouse was systematically adjusted to 10. For some experiments, pups were separated from the lactating female 4 h before being killed in order to limit milk secretion by MESCs (Wilde *et al.*, 1999; Weaver and Hernandez, 2016). Mice were killed by cervical dislocation at day 10 of lactation,

Antibody	Supplier	WB	IIF
β-Actin	Sigma-Aldrich	1:5000	x
PLIN2/adipophilin	Progen	1:5000	1:100
Annexin A2	Gift from J. Ayala-Sanmartin	1:500	1:50
ARK2/Aurora	Gift from N. Beaujean; Santa Cruz Biotechnology	x	1:50
Butyrophilin	Gift from I. H. Mather	1:3000	1:300
Calnexin	Enzo Life Sciences	1:1000	x
Mouse caseins (#7781)	Gift from M. C. Neville	x	1:50
Caveolin1	BD Transduction Laboratories	1:1000	1:100
E-cadherin	BD Transduction Laboratories	1:2000	x
Erlin2	Sigma-Aldrich	1:1000	x
Flotillin2	Santa Cruz Biotechnology	1:1000	x
GM130	BD Transduction Laboratories	1:250	x
GRP78/BiP	Abcam	1:1000	1:150
Mucin1	Abcam	1:500	1:100
C23/nucleolin	Gift from N. Beaujean; Santa Cruz Biotechnology	x	1:20
PDIA3	Abcam	1:500	1:100
Rab7	Gift from M. Zerial	1:250	1:50
Rab18	Calbiochem	1:1000	1:50
Sec22b	Synaptic Systems	1:5000	1:100
Syntaxin 3	Synaptic Systems	1:500	1:150
Syntaxin 4	Chemicon International	1:300	1:50
Syntaxin 6	Gift from S. Tooze	1:1000	1:50
Syntaxin 7	Synaptic Systems	1:1000	1:100
Syntaxin 12	Synaptic Systems	1:1000	1:100
Syntaxin 18	Synaptic Systems	1:1500	x
VAMP4	Abcam	1:500	1:50
VAMP8	Novus Biologicals	1:200	1:25

BiP, binding immunoglobulin protein; GRP, glucose-regulated protein; PDI, protein disulfide isomerase; PLIN2, perilipin; SNAP23, synaptosomal-associated protein; VAMP, vesicle-associated membrane protein; x, not used.

TABLE 1: Antibodies used for Western blot and indirect immunofluorescence experiments.

and the inguinal mammary glands were immediately excised. All ethical aspects of animal care complied with relevant guidelines and licensing requirements laid down by the French Ministry of Agriculture, and the procedures used were approved by the local ethics committee (Agreement 12/097 from the *Comethea* Jouy-en-Josas/AgroParisTech).

Antibodies

Primary antibodies and the dilutions used for indirect immunofluorescence (IIF) and Western blot (WB) experiments are given in Table 1. The antibodies against mouse caseins (7781), Stx-6, butyrophilin, Rab7, annexin A2 (AnxA2), C23/nucleolin, and ARK2/Aurora were generous gifts from M. C. Neville (University of Colorado Health Sciences Center, Aurora, CO), S. Tooze (Cancer Research UK, London Research Institute, London, United Kingdom), I. H. Mather (Department of Animal and Avian Sciences, University of Maryland, College Park, MD), M. Zerial (Max Planck Institute for Molecular Cell Biology and Genetics, Dresden, Germany), J. Ayala-Sanmartin (CNRS, UMR7203, Laboratoire des Biomolécules, Ecole Normale Supérieure, Paris, France), and N. Beaujean (UMR1198 Biologie du Développement et Reproduction, INRA, Jouy-en-Josas, France), respectively. With the exception of the anti-PLIN2, produced in guinea pig, and the anti-flotillin2, produced in mouse, all primary antibodies used were developed in rabbit. Secondary antibodies used in IIF experiments were tetramethylrhodamine isothiocyanate– or fluorescein isothiocyanate (FITC)–conjugated goat anti-rabbit immunoglobulin G (IgG) (H + L) (1:300 dilution; Jackson ImmunoResearch Laboratories, Interchim, Montluçon, France, and Santa Cruz Biotechnology, Tebu-Bio, Le Perray-en-Yveline, France, respectively) and rhodamine-conjugated goat anti-guinea pig IgG (H + L) (1:300 dilution; Santa Cruz Biotechnology). For WB experiments, the secondary antibodies were horseradish peroxidase (HRP)–conjugated goat anti-rabbit IgG (1:5000 dilution; Jackson ImmunoResearch Laboratories), HRP-conjugated goat anti-guinea pig IgG (1:5000 dilution; Santa Cruz Biotechnology), or HRP-conjugated sheep anti-mouse pIgG (1:2000 dilution; Sigma-Aldrich, Lyon, France).

Mouse milk collection

At day 10 of lactation (L10), pups were separated from their mothers 4 h before milking. Dams were intraperitoneally injected with 0.2 U

of synthetic oxytocin (CEVA Santé Animale, Libourne, France) and anesthetized (0.01 ml/g of body weight) with a solution of 10% Imalgene 1000 (Merial, Lyon, France) and 5% Rompun (Bayer Pharma, Puteaux, France) in saline. Mouse milk was manually collected in a sterile tube kept on ice and eventually stored at –80°C for MFGM protein preparation. For WB analysis, milk samples were diluted with water in a 1:4 (vol:vol) ratio, skimmed by centrifugation (10,000 × *g*, 4°C, 15 min), and stored at –80°C.

Preparation of mammary acini

Mammary acini were prepared from mice at L10 as previously described (Chat *et al.*, 2011). Tissue digestion was controlled by direct observation of the preparation under a microscope. Mammary acini were thoroughly rinsed with DMEM/F12 to remove collagenase A and recovered by low-speed centrifugation.

CLD and MFGM preparation

Unless specified, all procedures were performed at 4°C. CLDs were extracted from freshly prepared acini purified from mouse mammary glands (at least four animals) at L10 using a procedure adapted from Liu *et al.* (2008). Briefly, cells were washed in ice-cold PBS, resuspended, and mechanically homogenized in buffer A (25 mM tricine, pH 7.6, 2 mM EDTA, 2 mM $MgCl_2$, 250 mM sucrose) containing 0.5 mM phenylmethylsulfonyl fluoride (PMSF) and a protease inhibitor cocktail (1:50 dilution; Sigma-Aldrich). We added 6 ml of the homogenate to an SW41 tube and loaded 6 ml of buffer B (20 mM 4-(2-hydroxyethyl)-1-piperazineethanesulfonic acid, pH 7.4, 100 mM KCl, 2 mM $MgCl_2$, 0.5 mM PMSF) on top of the postnuclear supernatant fraction. After centrifugation at 274,000 × *g* for 1 h at 4°C, the tubes were placed at –20°C for 24 h. CLDs were carefully collected from the top layer of the frozen gradient and washed three times with buffer B. CLD proteins were quantified using a Bradford assay. Quality of the CLD preparation was controlled by light and fluorescence microscopy using BODIPY 493/503 (Molecular Probes), Alexa 594–conjugated cholera toxin B subunit (CTxB; Invitrogen), Alexa Fluor 594–conjugated WGA, or rhodamine-conjugated phalloidin (Molecular Probes) to label neutral lipids, GM1 ganglioside, glycoconjugates, or F-actin, respectively.

MFGMs were prepared from mouse milk collected at L10 (milk from at least two animals was pooled for each preparation) according to the procedures described by Fortunato *et al.* (2003) and Spertino *et al.* (2012). Briefly, whole mouse milk was diluted 1:4 in sterile water and centrifuged at 10,000 × *g* for 15 min at 4°C, and the cream was manually collected from the top of the tube. Skimmed milk was centrifuged at 13,000 × *g* for 15 min at room temperature to obtain the lactoserum and the caseins in the pellet. For protein extraction, the cream was washed by three cycles of dispersion in 0.9% (wt/vol) NaCl, followed by centrifugation at 4000 × *g* for 30 min at room temperature to remove residual caseins and whey proteins eventually adsorbed to fat globules. The lysis of MFGs was performed in 63 mM Tris-HCl, pH 6.8, containing 2% SDS, 5% β-mercaptoethanol (β-MeOH), and protease and phosphatase inhibitor cocktails for 1 h at room temperature and with regular vortexing. Lysate was centrifuged at 10,000 × *g* for 10 min at room temperature, and proteins present in the supernatant were precipitated with 10% trichloroacetic acid at 4°C for 1 h, pelleted at 13,000 × *g* for 30 min, and resuspended in ethanol/ether (vol/vol) before centrifugation at 13,000 × *g* for 10 min at 4°C. The final pellet was solubilized in a buffer containing 62 mM Tris-HCl, pH 6.8, 10% glycerol (wt/vol), 10 mM EDTA, 3% SDS, and 3% β-MeOH, boiled for 5 min, and stored at –20°C until SDS–PAGE analysis. Protein quantification was performed using the BCA Protein Assay Kit (Pierce Perbio, Villebon-sur-Yvette, France) on 20 µl of MFGM proteins precipitated with acetone and resuspended in water. The quality of both CLD and MFGM preparations was controlled by direct microscopic observation of the purified structures after fluorescent labeling with BODIPY 493/503 (Molecular Probes) and by analyzing specific marker proteins by WB.

LC-MS/MS

For MS analysis, samples (~8 µg) were resolved on 4–12% polyacrylamide gels (NuPAGE Novex, 4–12% Bis-Tris gel, NP002) in 2-(*N*-morpholino)ethanesulfonic acid (MES) buffer and stained with SimplyBlue SafeStain G250 (LC6060; Invitrogen). The molecular mass of the detected proteins was evaluated by comparison with PageRuler Prestained Protein Ladder (Euromedex, Souffelweyersheim, France) or See Blue Plus 2 (Invitrogen) markers. Twenty-six slices covering the whole gel lane were excised and placed in the wells of a 96-well plate. The pieces of gel were washed twice with successive baths of 50 M NH_4HCO_3/acetonitrile (ACN; 50/50; vol/vol). Gel pieces were dried, and proteins were reduced using 10 mM dithiothreitol in 25 mM NH_4HCO_3, followed by alkylation with 55 mM iodoacetamide in 25 mM NH_4HCO_3. Digestion was subsequently performed for 6 h at 37°C with 100 ng of modified trypsin (Promega, Madison, WI) in 50 mM NH_4HCO_3. The peptides were extracted with 2% trifluoroacetic acid (TFA), 50% ACN, and ACN successively. The peptide extracts and the supernatants from the digestion were pooled and dried in a vacuum centrifuge and then resuspended in 20 µl of 0.08% TFA and 2% ACN. HPLC was performed on an Ultimate 3000 LC system (Dionex, Thermo Fisher Scientific). A 4-µl sample was loaded at 20 µl/min on a precolumn cartridge (stationary phase: C18 PepMap 100, 5 µm; column: 300 µm inner diameter [i.d.], 5 mm; Dionex) and desalted with 0.08% TFA and 2% ACN. After 4 min, the precolumn cartridge was connected to the separating PepMap C18 column (stationary phase: C18 PepMap 100, 3 µm; column: 75 µm i.d., 150 mm; Dionex). The buffers were 0.1% HCOOH/2% ACN (A) and 0.1% HCOOH/80% ACN (B). The peptide separation was achieved with a linear gradient from 0 to 36% B for 18 min at 300 nl/min. One run took 50 min or 140 min, including the regeneration step at 100% B and the equilibration step at 100% A. The eluted peptides were analyzed online with an LTQ-Orbitrap mass spectrometer (Thermo Fisher Scientific, Villebon-sur-Yvette, France) using a nanoelectrospray interface. Ionization (1.3-kV ionization potential) was performed with a liquid junction and a capillary probe (10-µm i.d.; NewObjective). Peptide ions were analyzed using Xcalibur 2.07 with the following data-dependent acquisition steps: 1) full MS scan in orbitrap (mass-to-charge ratio [*m/z*] = 300–1600, profile mode) and 2) MS/MS in linear trap (*qz* = 0.25; activation time, 30 ms; collision energy, 45%; centroid mode). Step 2 was repeated for the four major ions detected in step 1. Dynamic exclusion time was set to 90 s.

Peptide identification and data analysis

A database search was performed with X!Tandem (v2010.12.01.1; www.thegpm.org/TANDEM/) using the X!Tandem pipeline (version 3.1.3; pappso.inra.fr/bioinfo/xtandempipeline/). The enzymatic cleavage was declared to be a trypsin digestion with one possible miscleavage. Cys carboxyamidomethylation and Met oxidation were set to static and possible modifications, respectively. Precursor mass and fragment mass tolerance were 10 ppm and 0.5 Da, respectively. A refinement search was performed with similar parameters, except that semitryptic peptides and possible N-ter protein acetylation were searched. Several databases were used: the Uniprot KB *Mus musculus*, C57BL6 database (49,728 entries, version March 2011 from EBI [www.ebi.ac.uk/integr8]) and the contaminant

database (trypsin, keratins, etc.). The identified proteins were filtered according to the following restrictions: 1) a minimum of two different peptides was required with an *E* value <0.05, and 2) a protein *E* value (product of unique peptide *E* values) $<10^{-4}$. The mass spectrometry proteomics data have been deposited with the ProteomeXchange Consortium (Vizcaíno *et al.*, 2014) via the PRIDE partner repository with the data set identifier PXD001024 and DOI 10.6019/PXD001024. For further analysis, only the specific protein isoforms (difference of at least two peptides) from the groups identified by LC-MS/MS were manually annotated in the context of GO to assign them a unique relevant function and cellular localization. When necessary, a probable cellular localization was assigned to some proteins based on bibliographic data or on their amino acid sequence using PsortII prediction software (psort.hgc.jp/form2.html). All of the MS data were statistically analyzed using the proportion test of R software (R Development Core Team, 2010; www.R-project.org).

Western blot

A 20-µg amount of total protein from the MFGM fractions was analyzed by SDS-polyacrylamide 12% gel electrophoresis (SDS–PAGE) and transferred onto Hybond nitrocellulose membrane (Amersham). The membrane was blocked with 1% polyvinyl alcohol in PBS for 1 min and then with 10% nonfat milk in PBS/0.3% Tween 20 and incubated overnight with primary antibodies diluted as indicated in Table 1 in PBS with 1% milk and 0.3% Tween 20. The membrane was extensively washed with PBS/0.3% Tween 20 and incubated with HRP-conjugated goat anti-rabbit IgG (1:5000 dilution) or HRP-conjugated sheep anti-mouse IgG (1:5000 dilution) for 1 h at room temperature. The signal was detected by means of enhanced chemiluminescence (GE Healthcare, Orsay, France). The molecular mass of detected proteins was evaluated by comparison with the Prestained Protein Ladder (Euromedex). In some experiments, membranes were reprobed after stripping with Restore Western Blot Stripping Buffer (Pierce Perbio). Each experiment was repeated at least twice.

Immunofluorescence

Freshly collected mouse milk was centrifuged at 10,000 × *g* for 15 min at 4°C, and the cream fraction was fixed or not with 4% paraformaldehyde (PFA) in PBS for 15 min at 4°C and embedded in 20% gelatin in PBS. The gelatin blocks were immediately placed at 4°C for 30 min and at –20°C for 1 h and stored at –80°C. IIF was performed on 5-µm cryosections as described for mammary gland sections (see later description), except that the mounting medium was without 4,6-diamidino-2-phenylindole (DAPI).

Mammary gland fragments were prepared as described in Chat *et al.* (2011), except that they were fixed with 4% PFA in PBS for 15 min at room temperature. IIF was performed on tissue sections as indicated in Chat *et al*. (2011). Neutral lipids were stained with a solution of 3 µg/ml BODIPY 493/503 (Molecular Probes) diluted in PBS. Slides were mounted with Vectashield (Vector Laboratories LTD, United Kingdom) containing DAPI and stored at 4°C until observation. For some experiments, tissue sections or MFGs were also labeled for actin with rhodamine-conjugated phalloidin (Molecular Probes), GM1 ganglioside with Alexa 594–conjugated CTxB (Invitrogen), or free CH using filipin (Sigma-Aldrich). Each experiment was performed at least twice and included control sections incubated without primary antibody or with irrelevant primary antibodies (i.e., against nucleolin or ARK2/Aurora). Epifluorescence microscopy was performed with a Leica Leitz DMRB microscope equipped with standard filters for FITC, rhodamine, and DAPI emissions, a 63× oil-immersion objective (numerical aperture [NA] 1.3), and a DP50 imaging camera (Olympus, Rungis, France) coupled to the Cell˚F software (Olympus). Some images were captured with an optical sectioning microscope attached to an AxioObserver imaging Apotome system (Zeiss; 63×/NA 1.4 oil-immersion objective). Confocal microscopy was performed with a Zeiss LSM 510 microscope (Confocal Facilities, MIMA2 Platform, INRA Jouy-en-Josas, France; www6.jouy.inra.fr/mima2) equipped with CLSM 510 confocal laser scanning software, using a Plan-Apochromat 63× oil-immersion objective (NA 1.4) and the 488- or 568-nm excitation wavelength of the laser. All images were analyzed using ImageJ 1.47q software (Schneider *et al.*, 2012; http://rsb.info.nih.gov/ij/).

ACKNOWLEDGMENTS

We are grateful to P. Adenot from the INRA MIMA2 imaging core facility (INRA, Jouy-en-Josas, France), the staff of the IERP unit (UE 0907, INRA, Jouy-en-Josas, France), J. Castille for animal care and facilities, and the Plateau d'Analyse Protéomique par Séquençage et Spectrométrie de Masse (UMR 1319 MICALIS, INRA, Jouy-en-Josas, France) for analysis of our samples by MS. We also thank J. Ayala-Sanmartin, N. Beaujean, I. H. Mather, M. C. Neville, S. Tooze, and M. Zerial for providing very useful antibodies. We acknowledge N. Bouhmarou, C. Cébo, and A. Pauloin for technical help and advice, as well as K. Kiêu for help in statistical analysis of the data. We warmly thank E. Chanat for discussing some of the results and reading the first version of the manuscript and F. McAlpine and G. Wagman for critical reading of the manuscript.

REFERENCES

Affolter M, Grass L, Vanrobaeys F, Casado B, Kussmann M (2010). Qualitative and quantitative profiling of the bovine milk fat globule membrane proteome. J Proteomics 73, 1079–1088.

Barbosa AD, Savage DB, Siniossoglou S (2015). Lipid droplet-organelle interactions: emerging roles in lipid metabolism. Curr Opin Cell Biol 35, 91–97.

Bartz R, Li WH, Venables B, Zehmer JK, Roth MR, Welti R, Anderson RG, Liu P, Chapman KD (2007). Lipidomics reveals that adiposomes store ether lipids and mediate phospholipid traffic. J Lipid Res 48, 837–847.

Blanchette-Mackie EJ, Dwyer NK, Barber T, Coxey RA, Takeda T, Rondinone CM, Theodorakis JL, Greenberg AS, Londos C (1995). Perilipin is located on the surface layer of intracellular lipid droplets in adipocytes. J Lipid Res 36, 1211–1226.

Borgese N, Francolini M, Snapp E (2006). Endoplasmic reticulum architecture: structures in flux. Curr Opin Cell Biol 18, 358–364.

Bostrom P, Andersson L, Rutberg M, Perman J, Lidberg U, Johansson BR, Fernandez-Rodriguez J, Ericson J, Nilsson T, Boren J, *et al.* (2007). SNARE proteins mediate fusion between cytosolic lipid droplets and are implicated in insulin sensitivity. Nat Cell Biol 9, 1286–1293.

Bouchoux J, Beilstein F, Pauquai T, Guerrera IC, Chateau D, Ly N, Alqub M, Klein C, Chambaz J, Rousset M, *et al.* (2011). The proteome of cytosolic lipid droplets isolated from differentiated Caco-2/TC7 enterocytes reveals cell-specific characteristics. Biol Cell 103, 499–517.

Brasaemle DL, Dolios G, Shapiro L, Wang R (2004). Proteomic analysis of proteins associated with lipid droplets of basal and lipolytically stimulated 3T3-L1 adipocytes. J Biol Chem 279, 46835–46842.

Campbell-Valois FX, Trost M, Chemali M, Dill BD, Laplante A, Duclos S, Sadeghi S, Rondeau C, Morrow IC, Bell C, *et al.* (2012). Quantitative proteomics reveals that only a subset of the endoplasmic reticulum contributes to the phagosome. Mol Cell Proteomics 11, M111 016378.

Cebrian I, Visentin G, Blanchard N, Jouve M, Bobard A, Moita C, Enninga J, Moita LF, Amigorena S, Savina A (2011). Sec22b regulates phagosomal maturation and antigen crosspresentation by dendritic cells. Cell 147, 1355–1368.

Chamberlain LH, Gould GW (2002). The vesicle- and target-SNARE proteins that mediate Glut4 vesicle fusion are localized in detergent-insoluble lipid rafts present on distinct intracellular membranes. J Biol Chem 277, 49750–49754.

Chat S, Layani S, Mahaut C, Henry C, Chanat E, Truchet S (2011). Characterisation of the potential SNARE proteins relevant to milk product release by mouse mammary epithelial cells. Eur J Cell Biol 90, 401–413.

Chong BM, Russell TD, Schaack J, Orlicky DJ, Reigan P, Ladinsky M, McManaman JL (2011). The adipophilin C terminus is a self-folding membrane-binding domain that is important for milk lipid secretion. J Biol Chem 286, 23254–23265.
Collins RF, Schreiber AD, Grinstein S, Trimble WS (2002). Syntaxins 13 and 7 function at distinct steps during phagocytosis. J Immunol 169, 3250–3256.
Dai J, Sheetz MP (1995). Regulation of endocytosis, exocytosis, and shape by membrane tension. Cold Spring Harb Symp Quant Biol 60, 567–571.
Desjardins M (2003). ER-mediated phagocytosis: a new membrane for new functions. Nat Rev Immunol 3, 280–291.
Fortunato D, Giuffrida MG, Cavaletto M, Garoffo LP, Dellavalle G, Napolitano L, Giunta C, Fabris C, Bertino E, Coscia A, *et al.* (2003). Structural proteome of human colostral fat globule membrane proteins. Proteomics 3, 897–905.
Foster LJ, De Hoog CL, Mann M (2003). Unbiased quantitative proteomics of lipid rafts reveals high specificity for signaling factors. Proc Natl Acad Sci USA 100, 5813–5818.
Friedman JR, Voeltz GK (2011). The ER in 3D: a multifunctional dynamic membrane network. Trends Cell Biol 21, 709–717.
Fujimoto Y, Itabe H, Sakai J, Makita M, Noda J, Mori M, Higashi Y, Kojima S, Takano T (2004). Identification of major proteins in the lipid droplet-enriched fraction isolated from the human hepatocyte cell line HuH7. Biochim Biophys Acta 1644, 47–59.
Gao Q, Goodman JM (2015). The lipid droplet-a well-connected organelle. Front Cell Dev Biol 3, 49.
Garin J, Diez R, Kieffer S, Dermine JF, Duclos S, Gagnon E, Sadoul R, Rondeau C, Desjardins M (2001). The phagosome proteome: insight into phagosome functions. J Cell Biol 152, 165–180.
Goyette G, Boulais J, Carruthers NJ, Landry CR, Jutras I, Duclos S, Dermine JF, Michnick SW, LaBoissiere S, Lajoie G, *et al.* (2012). Proteomic characterization of phagosomal membrane microdomains during phagolysosome biogenesis and evolution. Mol Cell Proteomics 11, 1365–1377.
Guo W, Novick P (2004). The exocyst meets the translocon: a regulatory circuit for secretion and protein synthesis? Trends Cell Biol 14, 61–63.
Hatsuzawa K, Tamura T, Hashimoto H, Hashimoto H, Yokoya S, Miura M, Nagaya H, Wada I (2006). Involvement of syntaxin 18, an endoplasmic reticulum (ER)-localized SNARE protein, in ER-mediated phagocytosis. Mol Biol Cell 17, 3964–3977.
Heid HW, Keenan TW (2005). Intracellular origin and secretion of milk fat globules. Eur J Cell Biol 84, 245–258.
Hodges BD, Wu CC (2010). Proteomic insights into an expanded cellular role for cytoplasmic lipid droplets. J Lipid Res 51, 262–273.
Huston GE, Patton S (1990). Factors related to the formation of cytoplasmic crescents on milk fat globules. J Dairy Sci 73, 2061–2066.
Jagerstrom S, Polesie S, Wickstrom Y, Johansson BR, Schroder HD, Hojlund K, Bostrom P (2009). Lipid droplets interact with mitochondria using SNAP23. Cell Biol Int 33, 934–940.
Jahn R, Scheller RH (2006). SNAREs–engines for membrane fusion. Nat Rev Mol Cell Biol 7, 631–643.
Jeong J, Lisinski I, Kadegowda AK, Shin H, Wooding FB, Daniels BR, Schaack J, Mather IH (2013). A test of current models for the mechanism of milk-lipid droplet secretion. Traffic 14, 974–986.
Kiss RS, Nilsson T (2014). Rab proteins implicated in lipid storage and mobilization. J Biomed Res 28, 169–177.
Kralj M, Pipan N (1992). The role of exocytosis in the apocrine secretion of milk lipid globules in mouse mammary gland during lactogenesis. Biol Cell 75, 211–216.
Lang T (2007). SNARE proteins and "membrane rafts." J Physiol 585, 693–698.
Lingwood D, Simons K (2010). Lipid rafts as a membrane-organizing principle. Science 327, 46–50.
Liu P, Bartz R, Zehmer JK, Ying Y, Anderson RG (2008). Rab-regulated membrane traffic between adiposomes and multiple endomembrane systems. Methods Enzymol 439, 327–337.
Liu P, Ying Y, Zhao Y, Mundy DI, Zhu M, Anderson RG (2004). Chinese hamster ovary K2 cell lipid droplets appear to be metabolic organelles involved in membrane traffic. J Biol Chem 279, 3787–3792.
Loewen CJ, Roy A, Levine TP (2003). A conserved ER targeting motif in three families of lipid binding proteins and in Opi1p binds VAP. EMBO J 22, 2025–2035.
Lopez C, Menard O (2011). Human milk fat globules: polar lipid composition and in situ structural investigations revealing the heterogeneous distribution of proteins and the lateral segregation of sphingomyelin in the biological membrane. Colloids Surf B Biointerfaces 83, 29–41.
Mather IH, Keenan TW (1998). Origin and secretion of milk lipids. J Mammary Gland Biol Neoplasia 3, 259–273.
McManaman JL (2012). Milk lipid secretion: recent biomolecular aspects. Biomol Concepts 3, 581–591.
McNew JA (2008). Regulation of SNARE-mediated membrane fusion during exocytosis. Chem Rev 108, 1669–1686.
Miller H, Castro-Gomes T, Corrotte M, Tam C, Maugel TK, Andrews NW, Song W (2015). Lipid raft-dependent plasma membrane repair interferes with the activation of B lymphocytes. J Cell Biol 211, 1193–1205.
Ogg SL, Weldon AK, Dobbie L, Smith AJ, Mather IH (2004). Expression of butyrophilin (Btn1a1) in lactating mammary gland is essential for the regulated secretion of milk-lipid droplets. Proc Natl Acad Sci USA 101, 10084–10089.
Ozeki S, Cheng J, Tauchi-Sato K, Hatano N, Taniguchi H, Fujimoto T (2005). Rab18 localizes to lipid droplets and induces their close apposition to the endoplasmic reticulum-derived membrane. J Cell Sci 118, 2601–2611.
Patton S, Huston GE (1988). Incidence and characteristics of cell pieces on human milk fat globules. Biochim Biophys Acta 965, 146–153.
Phillips MJ, Voeltz GK (2016). Structure and function of ER membrane contact sites with other organelles. Nat Rev Mol Cell Biol 17, 69–82.
Pisanu S, Ghisaura S, Pagnozzi D, Biosa G, Tanca A, Roggio T, Uzzau S, Addis MF (2011). The sheep milk fat globule membrane proteome. J Proteomics 74, 350–358.
Poston CN, Duong E, Cao Y, Bazemore-Walker CR (2011). Proteomic analysis of lipid raft-enriched membranes isolated from internal organelles. Biochem Biophys Res Commun 415, 355–360.
Prattes S, Horl G, Hammer A, Blaschitz A, Graier WF, Sattler W, Zechner R, Steyrer E (2000). Intracellular distribution and mobilization of unesterified cholesterol in adipocytes: triglyceride droplets are surrounded by cholesterol-rich ER-like surface layer structures. J Cell Sci 113, 2977–2989.
Prinz WA (2014). Bridging the gap: membrane contact sites in signaling, metabolism, and organelle dynamics. J Cell Biol 205, 759–769.
Puri N, Roche PA (2006). Ternary SNARE complexes are enriched in lipid rafts during mast cell exocytosis. Traffic 7, 1482–1494.
R Development Core Team (2010). R: A Language and Environment for Statistical Computing, Vienna: R Foundation for Statistical Computing.
Raucher D, Sheetz MP (2000). Cell spreading and lamellipodial extension rate is regulated by membrane tension. J Cell Biol 148, 127–136.
Reinhardt TA, Lippolis JD (2006). Bovine milk fat globule membrane proteome. J Dairy Res 73, 406–416.
Rusinol AE, Cui Z, Chen MH, Vance JE (1994). A unique mitochondria-associated membrane fraction from rat liver has a high capacity for lipid synthesis and contains pre-Golgi secretory proteins including nascent lipoproteins. J Biol Chem 269, 27494–27502.
Sakurai C, Hashimoto H, Nakanishi H, Arai S, Wada Y, Sun-Wada GH, Wada I, Hatsuzawa K (2012). SNAP-23 regulates phagosome formation and maturation in macrophages. Mol Biol Cell 23, 4849–4863.
Schneider CA, Rasband WS, Eliceiri KW (2012). NIH Image to ImageJ: 25 years of image analysis. Nat Methods 9, 671–675.
Schrader M, Godinho LF, Costello JL, Islinger M (2015). The different facets of organelle interplay-an overview of organelle interactions. Front Cell Dev Biol 3, 56.
Shoshan-Barmatz V, Zalk R, Gincel D, Vardi N (2004). Subcellular localization of VDAC in mitochondria and ER in the cerebellum. Biochim Biophys Acta 1657, 105–114.
Simons K, Sampaio JL (2011). Membrane organization and lipid rafts. Cold Spring Harb Perspect Biol 3, a004697.
Sollner T, Bennett MK, Whiteheart SW, Scheller RH, Rothman JE (1993a). A protein assembly-disassembly pathway in vitro that may correspond to sequential steps of synaptic vesicle docking, activation, and fusion. Cell 75, 409–418.
Sollner T, Whiteheart SW, Brunner M, Erdjument-Bromage H, Geromanos S, Tempst P, Rothman JE (1993b). SNAP receptors implicated in vesicle targeting and fusion. Nature 362, 318–324.
Spertino S, Cipriani V, De Angelis C, Giuffrida MG, Marsano F, Cavaletto M (2012). Proteome profile and biological activity of caprine, bovine and human milk fat globules. Mol Biosyst 8, 967–974.
Staubach S, Razawi H, Hanisch FG (2009). Proteomics of MUC1-containing lipid rafts from plasma membranes and exosomes of human breast carcinoma cells MCF-7. Proteomics 9, 2820–2835.
Stone SJ, Levin MC, Zhou P, Han J, Walther TC, Farese RV Jr (2009). The endoplasmic reticulum enzyme DGAT2 is found in mitochondria-associated membranes and has a mitochondrial targeting signal that promotes its association with mitochondria. J Biol Chem 284, 5352–5361.

Tauchi-Sato K, Ozeki S, Houjou T, Taguchi R, Fujimoto T (2002). The surface of lipid droplets is a phospholipid monolayer with a unique fatty acid composition. J Biol Chem 277, 44507–44512.
Truchet S, Chat S, Ollivier-Bousquet M (2014). Milk secretion: the role of SNARE proteins. J Mammary Gland Biol Neoplasia 19, 119–130.
Turner MD, Rennison ME, Handel SE, Wilde CJ, Burgoyne RD (1992). Proteins are secreted by both constitutive and regulated secretory pathways in lactating mouse mammary epithelial cells. J Cell Biol 117, 269–278.
Turro S, Ingelmo-Torres M, Estanyol JM, Tebar F, Fernandez MA, Albor CV, Gaus K, Grewal T, Enrich C, Pol A (2006). Identification and characterization of associated with lipid droplet protein 1: a novel membrane-associated protein that resides on hepatic lipid droplets. Traffic 7, 1254–1269.
Vizcaíno JA, Deutsch EW, Wang R, Csordas A, Reisinger F, Ríos D, Dianes JA, Sun Z, Farrah T, Bandeira N, Binz PA, *et al.* (2014). ProteomeXchange provides globally co-ordinated proteomics data submission and dissemination. Nat Biotechnol 223–226.
Vorbach C, Scriven A, Capecchi MR (2002). The housekeeping gene xanthine oxidoreductase is necessary for milk fat droplet enveloping and secretion: gene sharing in the lactating mammary gland. Genes Dev 16, 3223–3235.
Wan HC, Melo RC, Jin Z, Dvorak AM, Weller PF (2007). Roles and origins of leukocyte lipid bodies: proteomic and ultrastructural studies. FASEB J 21, 167–178.
Wang CC, Shi H, Guo K, Ng CP, Li J, Gan BQ, Chien Liew H, Leinonen J, Rajaniemi H, Zhou ZH, *et al.* (2007). VAMP8/endobrevin as a general vesicular SNARE for regulated exocytosis of the exocrine system. Mol Biol Cell 18, 1056–1063.
Wang W, Lv N, Zhang S, Shui G, Qian H, Zhang J, Chen Y, Ye J, Xie Y, Shen Y, *et al.* (2012). Cidea is an essential transcriptional coactivator regulating mammary gland secretion of milk lipids. Nat Med 18, 235–243.
Weaver SR, Hernandez LL (2016). Autocrine-paracrine regulation of the mammary gland. J Dairy Sci 99, 842–853.
Weber T, Zemelman BV, McNew JA, Westermann B, Gmachl M, Parlati F, Sollner TH, Rothman JE (1998). SNAREpins: minimal machinery for membrane fusion. Cell 92, 759–772.
Westrate LM, Lee JE, Prinz WA, Voeltz GK (2015). Form follows function: the importance of endoplasmic reticulum shape. Annu Rev Biochem 84, 791–811.
Wilde CJ, Knight CH, Flint DJ (1999). Control of milk secretion and apoptosis during mammary involution. J Mammary Gland Biol Neoplasia 4, 129–136.
Wilfling F, Haas JT, Walther TC, Farese RV Jr (2014). Lipid droplet biogenesis. Curr Opin Cell Biol 29, 39–45.
Wooding FB (1971). The mechanism of secretion of the milk fat globule. J Cell Sci 9, 805–821.
Wooding FB, Peaker LJ (1970). Theories of milk secretion: evidence from e electron microscopic examination of milk. Nature 226, 762–764.
Wooding FB, Sargeant TJ (2015). Immunocytochemical evidence for Golgi vesicle involvement in milk fat globule secretion. J Histochem Cytochem 63, 943–951.
Wu CC, Howell KE, Neville MC, Yates JR 3rd, McManaman JL (2000). Proteomics reveal a link between the endoplasmic reticulum and lipid secretory mechanisms in mammary epithelial cells. Electrophoresis 21, 3470–3482.
Yu MJ, Pisitkun T, Wang G, Aranda JF, Gonzales PA, Tchapyjnikov D, Shen RF, Alonso MA, Knepper MA (2008). Large-scale quantitative LC-MS/MS analysis of detergent-resistant membrane proteins from rat renal collecting duct. Am J Physiol Cell Physiol 295, C661–678.
Zhai J, Strom AL, Kilty R, Venkatakrishnan P, White J, Everson WV, Smart EJ, Zhu H (2009). Proteomic characterization of lipid raft proteins in amyotrophic lateral sclerosis mouse spinal cord. FEBS J 276, 3308–3323.